Am J Cancer Res 2020;10(2):545-563
www.ajcr.us /ISSN:2156-6976/ajcr0107920

Original Article

Trifluoperazine prolongs the survival of experimental brain metastases by STAT3-dependent lysosomal membrane permeabilization

Xin Zhang[1,2,3], Kaikai Ding[2,5], Jianxiong Ji[1,2], Himalaya Parajuli[3], Synnøve Nymark Aasen[3], Heidi Espedal[3,4], Bin Huang[1,2], Anjing Chen[1,2], Jian Wang[1,2,3], Xingang Li[1,2], Frits Thorsen[1,2,3,4]

[1]Department of Neurosurgery, Qilu Hospital of Shandong University and Brain Science Research Institute, Shandong University, Jinan, China; [2]Shandong Key Laboratory of Brain Function Remodeling, China; [3]Department of Biomedicine, [4]Molecular Imaging Center, University of Bergen, Bergen, Norway; [5]Department of Radiation Oncology, Qilu Hospital of Shandong University, Jinan 250012, China

Received January 15, 2020; Accepted January 23, 2020; Epub February 1, 2020; Published February 15, 2020

Abstract: Brain metastasis is a major cause of mortality in melanoma patients. The blood-brain barrier (BBB) prevents most anti-tumor compounds from entering the brain, which significantly limits their use in the treatment of brain metastasis. One strategy in the development of new treatments is to assess the anti-tumor potential of drugs currently used in the clinic. Here, we tested the anti-tumor effect of the BBB-penetrating antipsychotic trifluoperazine (TFP) on metastatic melanoma. H1 and Melmet1 human metastatic melanoma cell lines were used in vitro and in vivo. TFP effects on viability and toxicity were evaluated in proliferation and colony formation assays. Preclinical, therapeutic efficacy was evaluated in NOD/SCID mice, after intracardial injection of tumor cells. Molecular studies using immunohistochemistry, western blots, immunofluorescence and transmission electron microscopy were used to gain mechanistic insight into the biological activity of TFP. Our results showed that TFP decreased cell viability and proliferation, colony formation and spheroid growth in vitro. The drug also decreased tumor burden in mouse brains and prolonged animal survival after injection of tumor cells (53.0 days vs 44.5 days), TFP treated vs untreated animals, respectively ($P < 0.01$). At the molecular level, TFP treatment led to increased levels of LC3B and p62 in vitro and in vivo, suggesting an inhibition of autophagic flux. A decrease in LysoTracker Red uptake after treatment indicated impaired acidification of lysosomes. TFP caused accumulation of electron dense vesicles, an indication of damaged lysosomes, and reduced the expression of cathepsin B, a main lysosomal protease. Acridine orange and galectin-3 immunofluorescence staining were evidence of TFP induction of lysosomal membrane permeabilization. Finally, TFP was cytotoxic to melanoma brain metastases based on the increased release of lactate dehydrogenase into media. Through knockdown experiments, the processes of TFP-induced lysosomal membrane permeabilization and cell death appeared to be STAT3 dependent. In conclusion, our work provides a strong rationale for further clinical investigation of TFP as an adjuvant therapy for melanoma patients with metastases to the brain.

Keywords: Trifluoperazine, melanoma brain metastases, STAT3, lysosomal membrane permeabilization

Introduction

Brain metastases are recognized as one of the main causes of mortality in patients with melanoma, occurring in more than 50% of melanoma patients during their course of the disease [1]. Treatment failure is thought to be due to their large size at the time of neurological presentation [2] and that they are highly radioresistant [3]. Thus, although management of melanoma brain metastases is comprehensive, typically including surgical resection, stereotactic radiosurgery, whole-brain radiotherapy (WBRT) and cytotoxic chemotherapy, prognosis remains poor, with a median patient survival of 4 to 5 months [4].

Targeted therapies, such as BRAF and MEK inhibitors, have been used in clinical trials [5], and have to some extent improved clinical outcome of melanoma patients with metastatic disease [6]. However, most of these patients will develop resistance to therapy within a few months [7]. Although recent advances in BRAF and immune checkpoint therapies to some extent have improved patient survival, the exis-

tence of the blood brain barrier (BBB) limits their penetrance into the brain [8] and thus, their efficacy in the treatment of brain metastasis. Molecules that penetrate the BBB more easily are therefore likely to improve treatment efficacy.

Autophagy is a lysosome-dependent process, in which metabolic wastes, toxic protein aggregates, nonfunctional organelles and intracellular pathogens are degraded for recycling [9]. The lysosome, one of the cytoplasmic membrane-bound organelles, has previously been looked upon as a waste bag because of its roles in the late stage of autophagy [10]. Recently, several studies have shown that lysosomes may be involved in many other cellular processes, including regulation of cellular homeostasis [11]. It has also been demonstrated that lysosomes are involved in cell death, which is closely associated with lysosomal membrane permeabilization (LMP) [12]. Lysosomes contain more than 50 acidic hydrolases, which are critical for degradation [13]. LMP is a process in which destabilization of the lysosomal membrane causes leakage of lysosomal contents into the cytoplasm, ultimately resulting in cell death [14]. Among the lysosomal contents that lead to cell death, cathepsin B and D are the most important.

Trifluoperazine (TFP) has been used in the clinic for the treatment of schizophrenia for more than half a century. It is a typical antipsychotic compound of the phenothiazine chemical class, with a favorable size of 407.5 Da, enabling the drug to penetrate an intact BBB [15, 16]. Recent drug repurposing studies have shown that TFP has efficient anti-tumor effects in various tumor types, including lung cancer, malignant peripheral nerve sheath tumors and leukemia [17-19]. In a recent study, we demonstrated that TFP increased the radiosensitivity of glioblastoma (GBM) in vitro and in vivo, resulting in increased tumor cell death and prolonged animal survival [20]. However, we did not investigate a role for lysosomes in TFP-induced cell death.

In this study, we demonstrate that TFP has antitumor effects on melanoma brain metastases in vitro and in vivo, using a well-established animal model of experimental melanoma brain metastases. Furthermore, we demonstrate a relationship between the cytotoxic effects of TFP on melanoma brain metastases and LMP.

Materials and methods

Cell lines

The H1 and H3 cell lines were established in our laboratory from patient biopsies of human melanoma brain metastasis, as previously described [21, 22]. The Melmet 1 and Melmet 5 cell lines were obtained from Prof. Ø. Fodstad, University of Oslo, Norway. The H1 cells were transduced with two lentiviral vectors, encoding Dendra (a green fluorescent protein (GFP) variant) and luciferase to obtain the H1_DL2 cell line. The cell lines were cultured with DMEM supplemented with 10% heat-inactivated newborn calf serum, four times the prescribed concentration of non-essential amino acids, 2% L-glutamine, penicillin (100 IU/mL) and streptomycin (100 µL/mL; all reagents from Cambrex, East Rutherford, NJ, USA), hereafter named complete DMEM. Cells were incubated in a standard tissue culture incubator at 37°C, 100% humidity and 5% CO_2.

Cell viability assay

The H1, H3, Melmet 1 and Melmet 5 cell lines were suspended in complete DMEM and seeded (5×10^3 cells/well) into 96-well, flat-bottomed dishes (Nunc, Roskilde, Denmark). After incubation overnight at 37°C, cells were pretreated with PBS (control) or TFP (1-30 µM). After 24 h of culture, cells were incubated for an additional 2 h at 37°C with 100 µL of complete DMEM containing 0.1 mg/mL of Resazurin solution (Sigma-Aldrich, St. Louis, MO, USA), and absorbance was measured at a wavelength of at dual mode 560/590 nm with a scanning multiwell spectrophotometer (Victor 3 1420 multi-label counter, Perkin Elmer, Waltham, MA, USA). Each experiment was repeated 3 times.

Cell proliferation

Cell proliferation before and after treatment with TFP was studied using a cell counting assay. Briefly, H1 and Melmet 1 cells (2×10^4 cells/well) were plated in 12-well plates (Nunc). The cell monolayers were then treated with PBS (control), 3 µM or 6 µM TFP. On days 1, 2, 3 and 4 after treatment start, cells were trypsinized, stained with 0.4% trypan blue and counted. Growth curves were generated using GraphPad Prism 6 (GraphPad Software, Inc., San Diego, CA). Each experiment was repeated 3 times.

Colony formation assay

The H1, H3, Melmet 1 and Melmet 5 cells were each plated in six-well plates (Nunc, 3 × 10^3 cells/well). After treatment with PBS (control), 3 μM or 6 μM TFP for 24 h, the cells were rinsed in PBS 3 times and incubated with complete DMEM for 14 days. The colonies were then rinsed in PBS 3 times, fixed with 4% paraformaldehyde, rinsed with PBS 3 times, and stained with 0.1% crystal violet and counted. All colonies containing more than 50 cells were counted. Each experiment was repeated 3 times.

Spheroid growth

Multicellular spheroids from H1 and Melmet 1 cells were prepared as described below. Briefly, 3 × 10^3 cells in 100 μL of complete DMEM were seeded per well in Costar 96-well round bottom ultra-low attachment plates (Corning Inc., Corning, NY, USA). Cells were pelleted at 1000 × g for 15 min, and incubated for 5 days, after which they had rounded up into spheroids. The spheroids were exposed to PBS (control), 5 μM or 10 μM TFP for 15 days. Changes in two orthogonal spheroid diameters were measured for each spheroid using an IncuCyte Zoom live cell imaging system (Essen BioScience, Ann Arbor, MI, USA). Each experiment was repeated 3 times. For each cell line, 3 spheroids were measured per experiment.

Intracardial tumor cell injections and drug therapy

16 female NOD/SCID mice (6-8 weeks old) were anesthetized and fixed in a supine position on a heating pad to maintain a core temperature at 37°C. 5 × 10^5 H1_DL2 cells in 0.1 mL PBS were injected during 30 sec into the left cardiac ventricle of each mouse using a 30G insulin syringe (Omnican50, B. Brain Medical AS, Vestskogen, Norway), by ultrasound guidance (Vevo$^{(R)}$ 2100 Imaging System 230 V, Visual Sonics Inc., Toronto, Canada). After two weeks, the mice were randomized into two groups. The first group received TFP intraperitoneally (i.p.) 5 days/week (1 mg/kg in 100 mL PBS, 8 mice). The second group received 100 mL of PBS i.p. 5 days/week (control group, 8 mice).

Mice were euthanized if they showed weight loss of more than 20% of their body weight, or upon signs of severe neurological symptoms. The brains were harvested, fixed in 4% paraformaldehyde, and embedded in paraffin.

Magnetic resonance imaging (MRI)

Brain metastasis development in the NOD/SCID mice after intracardiac cell injection was studied using a 7 Tesla small-animal MR scanner (Bruker PharmaScan; Bruker BioSpin MRI, Ettlingen, Germany) equipped with a 1-channel circular transmitter coil and a 4-channel receiver surface coil. Coronal, T1 weighted (T1w) images were taken before and after injection of Omniscan contrast agent (GE Healthcare, Oslo, Norway), and images were produced with the following RARE sequence scan parameters: Field of view (FOV) 20 mm × 16 mm, matrix size 256 × 256, 0.5 mm slice thickness, repetition time (TR) 1000 ms, echo time (TE) 9 ms, flip angle (FA) 90°, 4 averages and scan time 3 min 12 sec. T2 weighted (T2w) coronal images were obtained with the following RARE sequence scan parameters: FOV 20 mm × 16 mm, matrix size 256 × 256, 0.5 mm slice thickness, TR 3200 ms, TE 38 ms, FA 90°, 4 averages, scan time 6 min 49 sec.

Visualization of MR images and quantification of tumor numbers and volumes (V = 4/3 × pi × r3) were performed using the 32-bit OsiriX freeware, version 5.8.1 (Pixmeo SARL, Geneva, Switzerland).

Immunohistochemical analysis

Paraffin-embedded mouse brain samples were sectioned (4 μm) and mounted onto microscopic slides. For histological assessment, sections were deparaffinized and stained with Hematoxylin and Eosin (H&E). For immunohistochemistry, deparaffinized sections were incubated with the primary antibody at 4°C overnight (LC3BI/II, 1:3200; Ki67, 1:800; P62, 1:250; all antibodies from Cell Signaling Technology, Beverly, MA, USA), rinsed with PBS, and incubated with goat anti-rabbit secondary antibody (ZSGB-Bio; Beijing, China). Three representative images from each section were taken under bright field microscopy (Leica DMi8, Leica Microsystems, Wetzlar, Germany). For each image, positively stained nuclei were counted using ImageJ software (V1.8.0, National Institutes of Health; Bethesda, MD, USA). Positively Ki67-stained cells are presented as a percentage of a total number of cells counted. Staining of cancer cells was scored as follows:

0, no staining; 1, weak staining in < 50% of cells; 2, weak staining in ≥ 50% of cells; 3, strong staining in < 50% of cells; and 4, strong staining in ≥ 50% of cells. For each group, 3 random mice were checked, and for each mouse, 3 images were obtained.

Western blot analysis

The H1, H3, Melmet 1 and Melmet 5 cell lines were grown in 6-well plates until the monolayers were 70-80% confluent. The cells were then treated with PBS (control), 3 μM or 6 μM TFP and incubated for 24 h. Cells were collected and whole-cell lysates (40 μg) were prepared from all cell lines using RIPA buffer (Thermo Fisher Scientific, Waltham, MA, USA). Proteins were resolved by sodium dodecyl sulfate-polyacrylamide gel electrophoresis and transferred to a polyvinylidene difluoride membrane. Membranes were blocked with 5% powdered skim milk dissolved in Tris-buffered saline (0.02 M Tris-HCl (pH 7.5), 0.15 M NaCl and 0.1% Tween20), and subsequently incubated with primary (Cell Signaling Technology) and indicated secondary antibodies (Thermo Fisher Scientific). Proteins on membranes were visualized using a chemiluminescence detection system, SuperSignal West Femto (Thermo Fisher Scientific), and imaged with the LAS-3000 image analysis system (Fujifilm, Tokyo, Japan). The following primary antibodies were used for western blot: GAPDH, LC3BI/II, P62, STAT3 and phosphorylated STAT3 (Tyr705).

Autophagic flux measurement

The Autophagy Tandem Sensor RFP-GFP-LC3B Kit (Thermo Fisher Scientific) enables monitoring of the various stages of autophagy through LC3B localization. The fluorescence from the sensor is based on the pH difference between the autolysosome and the autophagosome. By combining an acid-sensitive green fluorescent protein (GFP) with an acid insensitive red fluorescent protein (RFP), the change in LC3B localization from the autophagosomes (with a neutral pH) to the autolysosomes (with an acidic pH) can be visualized by imaging the specific loss of the GFP fluorescence, leaving only red fluorescence.

Briefly, cells were incubated with the RFP-GFP-LC3B reagent (2 μL/10,000 cells) in 24-well plates. After 48 h, cells were trypsinized, centrifuged, rinsed and cultured on coverslips in 24-well plates (1,000 cells/well). Cells were incubated overnight and then treated with 3 μM TFP or PBS for 24 h. Cells were fixed in 4% paraformaldehyde and antifade mounting medium (Thermo Fisher Scientific) was added. Images were captured using a Leica TCS SP5 confocal microscope (Leica Microsystems). Each experiment was repeated 3 times.

LysoTracker staining

LysoTracker Red (Thermo Fisher Scientific) was used as a probe for lysosomes to study potential changes in acidification and morphology after treatment. Following treatment with PBS (control) or 3 μM TFP for 24 h, H1 and Melmet 1 cells were treated with LysoTracker Red (final concentration of 66 nM). After incubation for 30 min at 37°C, cells were rinsed with PBS, and fixed with 4% paraformaldehyde at room temperature for 15 min. Antifade mounting medium (Thermo Fisher Scientific) was added, and the cells were imaged using a Leica TCS SP5 confocal microscope (Leica Microsystems). Each experiment was repeated 3 times, and 3 images were obtained in each group for each experiment.

Transmission electron microscopy (TEM)

TEM was used to study potential changes in the ultrastructure of cells after treatment. H1 and Melmet 1 cells treated with PBS (control) or 3 μM TFP for 24 h were fixed in 3% glutaraldehyde in PBS for 2 h, washed 5 times with 0.1 M cacodylate buffer, and post-fixed with 1% OsO4 in 0.1 M cacodylate buffer containing 0.1% CaCl2 for 1.5 h at 4°C. Cells were dehydrated in a graded alcohol series and embedded in epoxy resin. Ultra-thin sections were cut and stained with uranyl acetate and lead citrate. Images were taken using a JEM-1200EX II electron microscope (JEOL, Tokyo, Japan). Each experiment was repeated 3 times, and 3 images were obtained in each group for each experiment.

DQ-BSA uptake assay

A DQ-green-BSA dye was used to test lysosomal proteolytic degradation. H1 and Melmet 1 cells treated with PBS (control) or 3 μM TFP for 24 h were incubated with DQ-green-BSA (5 μg/mL, Invitrogen) at 37°C for 1 h. Cells were rinsed, fixed with 4% paraformaldehyde at room temperature for 15 min and stained with DAPI. Images were obtained using a Leica TCS SP5

confocal microscope (Leica Microsystems). Each experiment was repeated 3 times, and 3 images were obtained in each group for each experiment.

Cathepsin B activity assay

The Cathepsin B Activity Assay Kit (Abcam, Cambridge, UK) was used to test the activity of cathepsin B as described previously [20]. Briefly, after treatment with PBS (control) or 3 μM TFP for 24 h, cells were lysed in lysis buffer, and supernatants were incubated with cathepsin-B substrates (Ac-RR-AFC) at 37°C for 1.5 h. Fluorescence due to the cleaved substrate was measured on a scanning multiwell spectrophotometer (Victor 3 1420 multi-label counter, Perkin Elmer) at excitation/emission wavelengths = 400/505 nm. The results are represented as relative fluorescent units. Each experiment was repeated 3 times.

Lysosomal membrane stability

Lysosomal membrane stability was tested using acridine orange (AO; Sigma-Aldrich, USA) [23]. AO is a lysosomotropic weak base and will accumulate in acidic compartments. The concentration of AO is high in intact lysosomes, and emits red fluorescence. If the lysosomal membrane is impaired, AO concentrations are low, and emits green fluorescence. H1 and Melmet 1 cells were incubated with AO solution (5 μg/mL) in complete DMEM for 15 min at 37°C. Cells were exposed to PBS or 3 μM TFP for 60 min. Images were taken with a Leica TCS SP5 confocal microscope (Leica Microsystems). Each experiment was repeated 3 times, and 3 random images were taken in each group for each experiment.

Immunofluorescence

After treatment with PBS, 3 μM or 6 μM TFP for 24 h, H1 and Melmet 1 cells were rinsed 3 times with PBS, fixed with 4% paraformaldehyde at room temperature for 15 min and permeabilized with 0.2% Triton X-100 for 20 min. Cells were blocked with 5% BSA (Sigma), incubated with primary antibodies for galectin 3 (1:400, Cell Signaling Technology) or LAMP2 (1:100, Abcam, Cambridge, UK) overnight, and then stained with goat anti-rabbit IgG (Alexa Fluor 555, Thermo Fisher Scientific) for 1 h. Finally, the samples were mounted in mounting medium (Thermo Fisher Scientific). Three random fields were examined with a Leica TCS SP5 confocal microscope (Leica Microsystems). Each experiment was repeated 3 times.

Transfection of siRNA

H1 and Melmet 1 cells were transfected with siRNA using lipofectamine 2000 according to the manufacturer's protocol. The final concentration of siRNAs was 20 nM. Sequences for the siRNAs used were the following: control, 5'-UUCUCCGAACGUGUCACGUTT-3', STAT3, 5'-GUUCAUCUGUGUGACACCATT-3' (Genepharma, Shanghai, China). Western blot analysis was used to assess the knockdown efficiency of siRNA.

Lactate dehydrogenase (LDH) assay

Cell death was detected by measuring the release of LDH from the cytosol into the supernatant, using the Cytotoxicity Detection Kit (Roche Applied Science, Indianapolis, IN, USA) according to the manufacturer's instructions. After treatment with PBS, 6 μM TFP, 10 μM Pepstatin A, 20 nM siControl or 20 nM siSTAT3 for 48 h, H1 and Melmet 1 cells in each group were lysed with lysis buffer (2% Triton X-100). Supernatants were collected and measured at 490 nm on a scanning multiwell spectrophotometer (Victor 3 1420 multi-label counter, Perkin Elmer). In each group, the percentage cytotoxicity was calculated from the released LDH divided by the total amount of LDH. Each experiment was repeated 3 times.

Statistical analysis

Unpaired, two-tailed t-tests were performed using SPSS software v13.0 (SPSS Inc., Chicago, IL). Kaplan-Meier survival analysis and the Mantel-Cox log-rank test were performed in GraphPad Prism 6 (La Jolla, CA, USA), to assess survival differences between animal groups. Results are presented as the mean ± standard error (SE). *P*-values ≤ 0.05 were considered statistically significant.

Results

TFP treatment inhibits growth of melanoma brain metastatic cells in vitro

We first tested response to TFP on a panel of human metastatic melanoma cell lines using

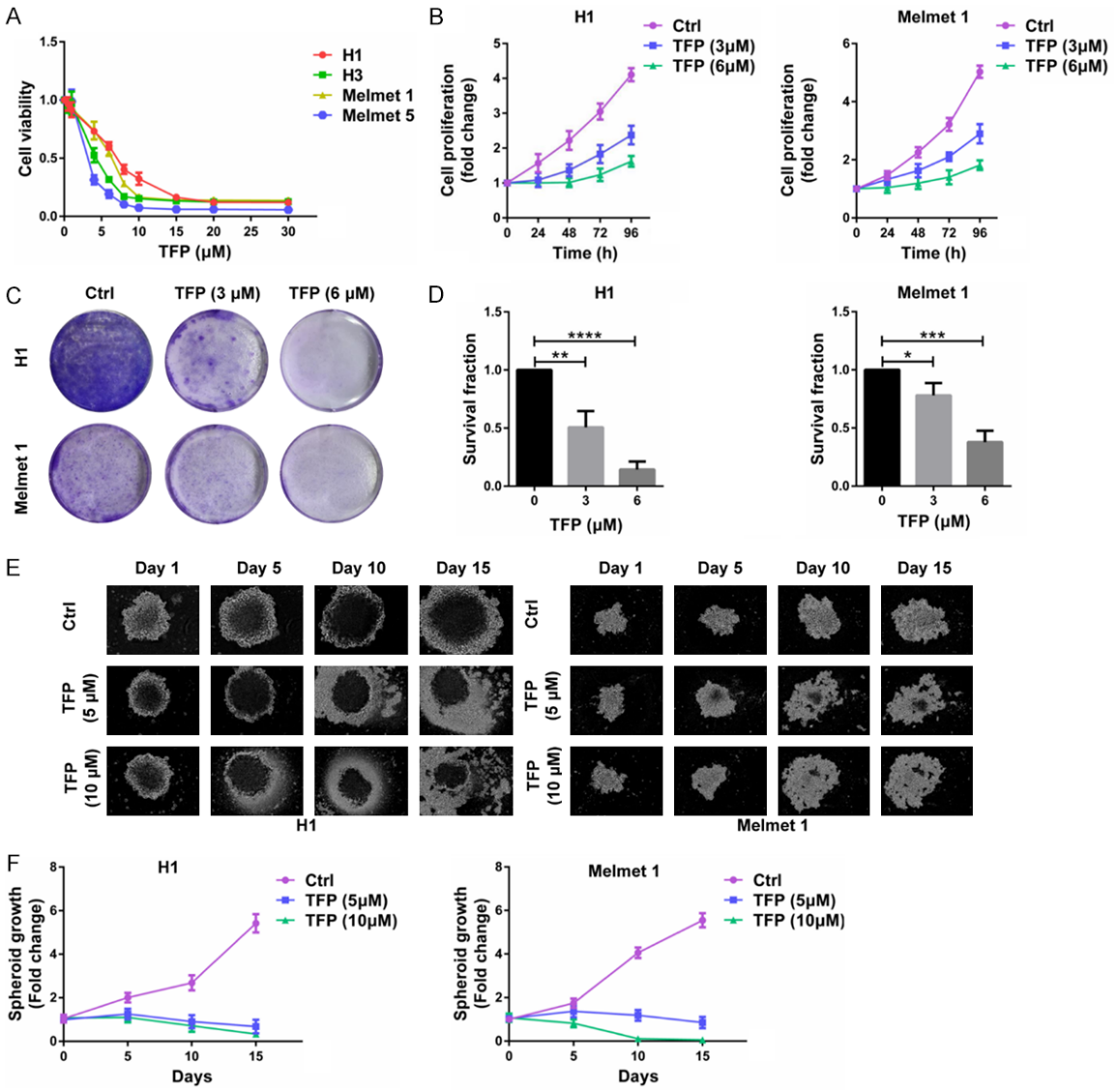

Figure 1. TFP inhibits *in vitro* growth of melanoma brain metastatic cells. (A) Cell viability of H1, H3, Melmet 1 and Melmet 5 cells after treatment with 0-30 μM TFP for 72 h. (B) Growth curves generated using cell counting for H1 and Melmet 1 cells over 96 h, after treatment with 0 μM (Ctrl), 3 μM or 6 μM TFP. (C) Image of colony formation assay for H1 and Melmet 1 cells at day 14, after pretreatment with 0 μM (Ctrl), 3 μM or 6 μM TFP for 24 h. (D) Quantification of the number of colonies seen in (C). *P < 0.05; **P < 0.01; ***P < 0.001; ****P < 0.0001. (E) Growth of multicellular spheroids derived from H1 and Melmet 1 cells, after treatment with 0 μM (Ctrl), 3 μM or 6 μM TFP for 15 days. (F) Quantification of fold-change in spheroid growth seen in (E).

several growth assays in vitro. First, increasing TFP concentrations decreased the cell viability of all 4 melanoma cell lines (**Figure 1A**), and the IC50 concentrations for the H1, H3, Melmet 1 and Melmet 5 cells were 7.2 μM, 4.1 μM, 6.5 μM and 3.3 μM, respectively. Second, growth curves generated with cell counting data demonstrated that cell proliferation was inhibited by TFP treatment relative to controls (**Figure 1B**). Third, colony formation was inhibited by TFP for all 4 cell lines (**Figures 1C**, **1D** and S1). TFP at 6 μM reduced colony number by > 50% relative to controls.

Finally, we examined the effect of TFP on 3D tumor spheroid growth. In a pilot study using 3 μM and 6 μM TFP, TFP at 3 μM was not able to inhibit spheroid growth (data not shown), likely due to low drug penetrance into the spheroids. We thus decided to use 5 μM and 10 μM for

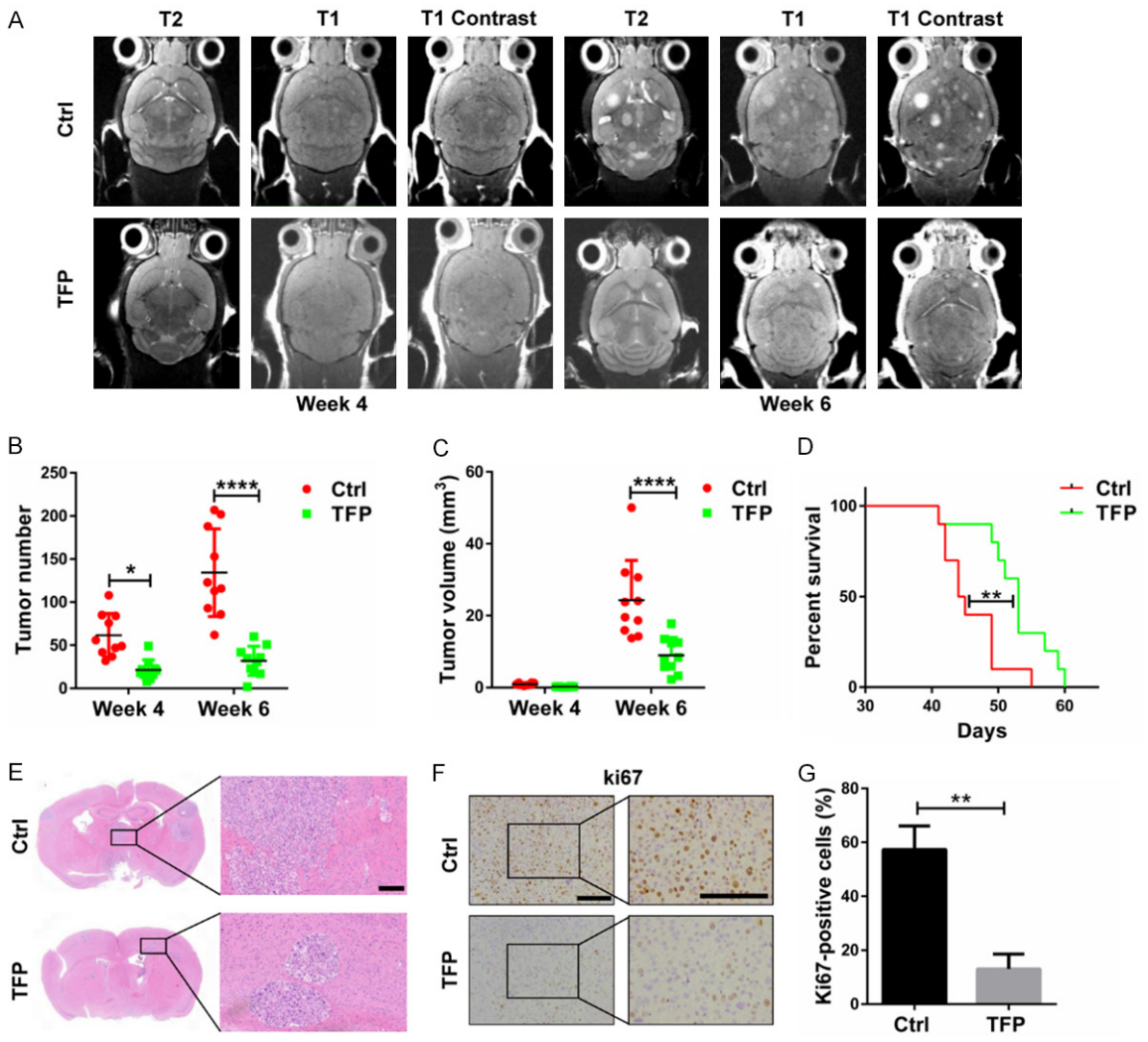

Figure 2. TFP decreases brain metastatic tumor burden *in vivo* and prolongs animal survival. (A) Development of H1_DL2 brain metastases assessed by T1-weighted (before and after contrast injections) and T2-weighted MRI at weeks 4 and 6 after intracardial tumor cell injections. Scale bar = 25 mm. (B) Quantification of the mean tumor numbers in controls and treated animals at weeks 4 and 6. *P < 0.05, ****P < 0.0001. (C) Quantification of the mean tumor volumes in controls and treated animals at weeks 4 and 6. ****P < 0.0001. (D) Kaplan-Meier survival plot for tumor bearing animals treated with TFP or vehicle control (Mantel-Cox log-rank test). **P < 0.01. (E) Images of H&E stained brain tumor sections of untreated (top row) or TFP treated (bottom row) mice. Scale bar = 100 µm. (F) Images of Ki-67 stained brain tumor sections of untreated (top row) or TFP treated (bottom row) mice. Scale bars = 100 µm. (G) Quantification of Ki-67 stained brain tumor sections. **P < 0.01.

this assay. At these concentrations, TFP significantly inhibited tumor spheroid growth over a 15-day time course (**Figure 1E** and **1F**).

TFP treatment decreases metastatic tumor burden in vivo and improves animal survival

Based on the in vitro results, we studied the anti-tumor effects of TFP in vivo using a well-established animal model of human melanoma brain metastasis [24]. MRI performed at weeks 4 and 6 after tumor cell injections, showed a significant decrease in total tumor numbers and total tumor volumes in the brains of TFP treated mice, as compared to untreated mice (**Figure 2A**). Quantification performed in OsiriX verified these results (**Figure 2B** and **2C**). TFP also improved animal survival, which was 53.0 days vs 44.5 days, TFP treated vs untreated animals, respectively (P < 0.01, **Figure 2D**).

H&E-stained sections of mouse brains confirmed that TFP treated mice exhibited fewer and smaller brain metastatic tumors compared to untreated mice (**Figure 2E**). Ki67 immunohistochemical staining of sections demonstrated

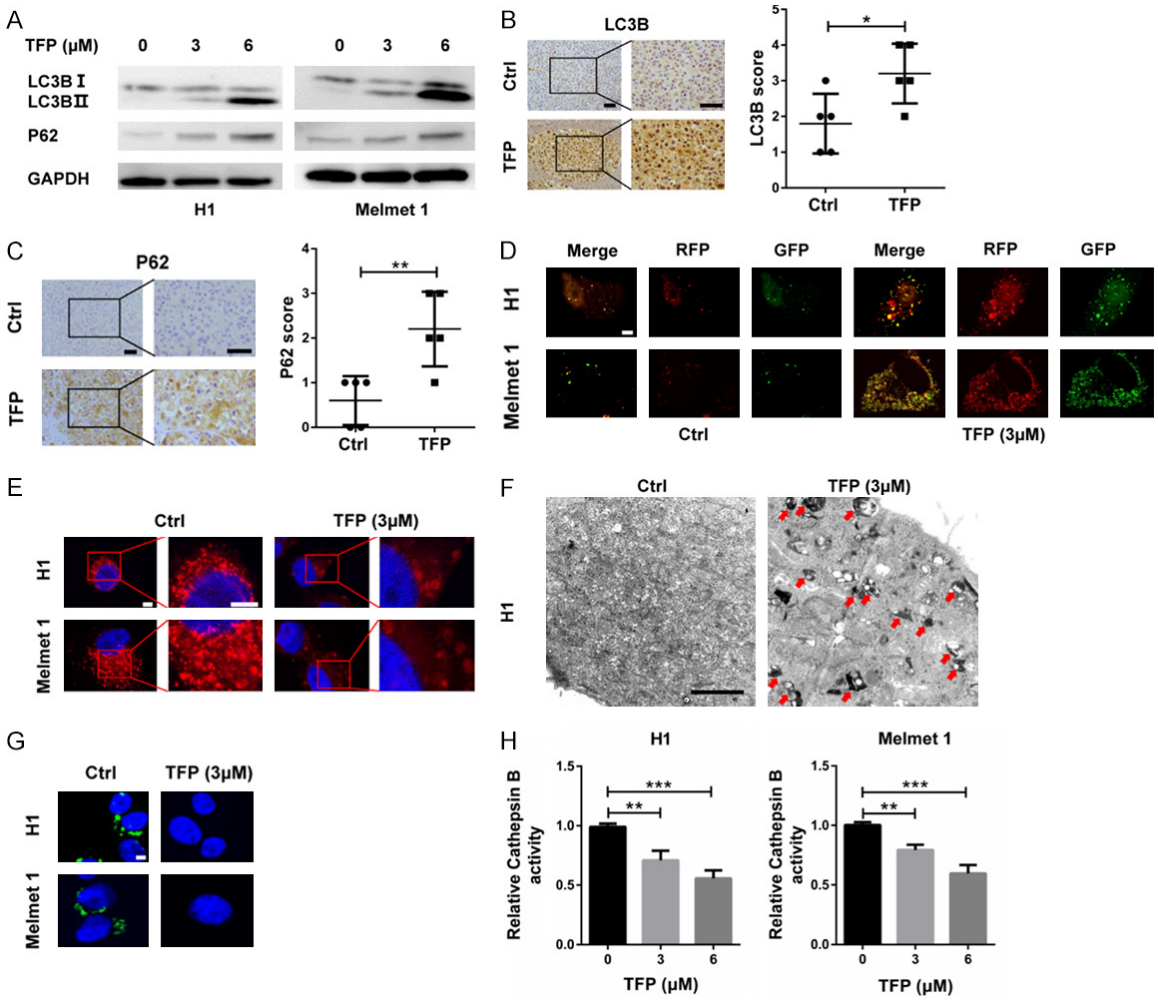

Figure 3. TFP inhibits autophagy in melanoma brain metastatic cells. (A) Western blot of LC3B, P62 and GAPDH (loading control) in H1 and Melmet 1 cells treated with 0 μM (Ctrl), 3 μM or 6 μM TFP for 24 h. Images of immunohistochemical staining and quantification of the expression of (B) LC3B and (C) P62 and in brain tumor sections from untreated (Ctrl) and TFP treated mice. Scale bars = 100 μm. *P < 0.05, **P < 0.01. (D) Confocal images of autophagic flux in H1 and Melmet 1 cells, as visualized with RFP-GFP-LC3, 48 h after treatment with either 0 μM (Ctrl) or 3 μM TFP. The increase in GFP (green) relative to RFP (red) after TFP treatment shows inhibition of autophagic flux. The quantification is shown in Figure S3. Scale bar = 10 μm. (E) Confocal images of lysosomes in H1 and Melmet 1 cells, stained with LysoTracker Red, 24 h after treatment with either 0 μM (Ctrl) or 3 μM TFP. Cell nuclei were counterstained with DAPI (blue). Scale bars = 10 μm. (F) Transmission electron micrographs, showing the ultrastructure of H1 cells treated with 0 mM (Ctrl) or 3 μM TFP. In TFP treated cells, electron dense vacuoles accumulated (red arrows). Scale bars = 1 μm. (G) Confocal images of the DQ-BSA uptake assay (green) in H1 and Melmet 1 cells. Cell nuclei were counterstained with DAPI (blue). Scale bar = 10 μm. (H) Quantification of the fluorometric assay, showing the relative cathepsin B activity in H1 and Melmet 1 cells treated with 0 μM (Ctrl), 3 μM or 6 μM TFP for 24 h. **P < 0.01, ***P < 0.001.

that tumor cell proliferation decreased under TFP treatment (57.33% ± 5.04% vs 13.00% ± 3.22% in untreated brain metastasis to in TFP treated brain metastasis; **Figure 2F** and **2G**, P < 0.01).

TFP treatment inhibits autophagy of melanoma brain metastatic cells

We have previously shown in GBM cell lines that one mechanism of TFP inhibition of cell growth is through inhibition of autophagy [20]. We therefore performed several assays to determine whether TFP also caused autophagy in human melanoma brain metastatic cells. Under TFP treatment, the levels of the autophagy related protein LC3B-II increased, as well as for P62, one of the most important long-lived proteins critical for the process (**Figures 3A** and S2). Immunohistochemical staining of brain sections from tumor bearing animals also dem-

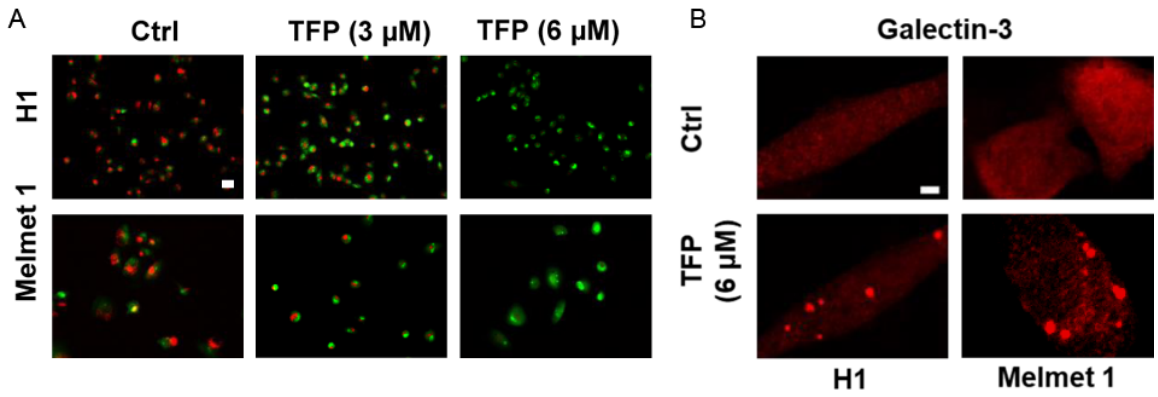

Figure 4. TFP treatment causes lysosomal membrane permeabilization in melanoma brain metastatic cells. (A) Confocal images of acridine orange staining to determine lysosomal membrane stability in H1 and Melmet 1 cells treated with 0 μM (Ctrl), 3 μM or 6 μM TFP for 60 min. The red fluorescence decreased after treatment with 3 μM or 6 μM TFP, indicating impaired lysosomal membranes. Scale bar = 50 μm. (B) Confocal images of immunofluorescence staining for galectin-3 in H1 and Melmet 1 cell lines, before and after treatment with 6 μM TFP for 24 h. In untreated cells, galectin-3 was distributed evenly in the cytoplasm, while in TFP-treated cells, galectin-3 was associated with punctate structures in the enlarged lysosomes. Scale bar = 10 μm.

onstrated that TFP treatment increased the expression of LC3B and P62 in brain metastases (**Figure 3B** and **3C**). Finally, using the RFP-GFP-LC3 probe, we found that the autophagic flux was interrupted after TFP treatment as there was no loss of GFP fluorescence indicating a shift to the lower pH autolysosome (**Figures 3D** and S3).

Next, we explored which phase of autophagic flux was inhibited. The upregulation of P62 may be due to TFP blocking either of two processes: the fusion of lysosomes with autophagosomes or the degradation of the autolysosomes. We used LysoTracker Red to stain the lysosomes before and after TFP treatment. Our results showed that in TFP treated cells, the intensity of red florescence decreased significantly compared to that in the control group. The lysosomes also changed morphologically, appearing to be enlarged (**Figure 3E**). Our results thus indicated that TFP interfered with the function of the lysosomes.

TEM was used to observe potential changes in the ultrastructure of tumor cells after TFP treatment. TFP caused accumulation of electron dense vesicles, which is consistent with damaged lysosomes (**Figures 3F** and S4). The morphological changes observed on TEM were further supported by results of the DQ-BSA uptake assay performed on cells in vitro. DQ-BSA is a substrate of lysosomal proteases, and the degradation of this substrate generates small particles with green florescence in functioning lysosomes. TFP treatment decreased green fluorescence, an indication of non-functioning lysosomes (**Figure 3G**).

Finally, the activity of cathepsin B, a critical lysosomal protease, was also reduced in TFP treated cells, as indicated by reduced GFP levels from the cleaved substrate Ac-RR-AFC after TFP treatment (**Figure 3H**). Taken together, our results demonstrated that TFP treatment impaired the function of lysosomes and as a result, autophagy was inhibited.

TFP treatment causes lysosomal membrane permeabilization in melanoma brain metastatic cells

The results from the LysoTracker Red experiments indicated that TFP treatment caused enlargement of lysosomes (**Figure 3E**).

Immunofluorescence staining with LAMP2, a lysosome-associated membrane protein, confirmed the accumulation of enlarged lysosomes in H1 and Melmet 1 cells under TFP treatment (Figure S5). The impaired function of the lysosomes in the presence of TFP (**Figure 3G** and **3H**) might further indicate that the drug causes lysosomal membrane permeabilization (LMP). Acridine orange staining, which detects intact membranes, decreased in TFP treated melanoma brain metastatic cells, demonstrating that lysosomal membranes had been compromised (**Figure 4A**).

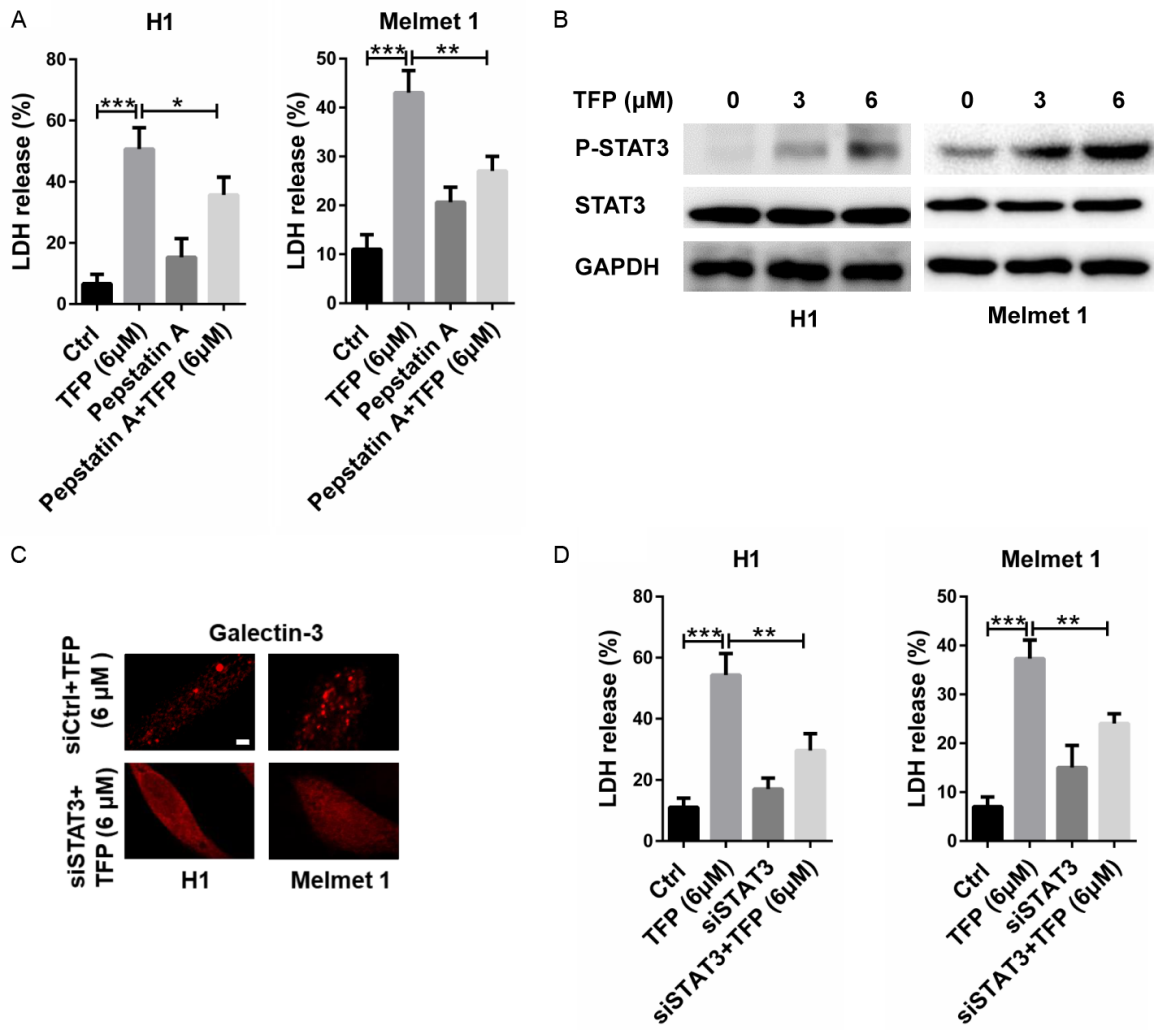

Figure 5. LMP-induced cell death is STAT3 dependent in melanoma brain metastatic cells. (A) LDH release in H1 and Melmet 1 cells, either untreated (Ctrl) cells, or after treatment with 6 μM TFP, 10 μM pepstatin A or combined treatment. (B) Western blot analysis of phosphorylated STAT3 after treatment of the H1 and Melmet 1 cells with 0 μM, 3 μM or 6 μM TFP for 24 h. (C) Confocal images of immunofluorescence staining for galectin-3 in the H1 and Melmet 1 cell lines, treated with 6 μM TFP+siCtrl or 6 μM TFP+siSTAT3 for 24 h. LMP is inhibited after STAT3 knockdown. Scale bar = 10 μm. (D) LDH release in H1 and Melmet 1 cells, either untreated cells (Ctrl), or cells treated with 6 μM TFP, siSTAT3 or combined treatment. siSTAT3+TFP treatment reduced LDH release compared to TFP treatment alone. *P < 0.05, **P < 0.01, ***P < 0.001.

We also examined the integrity of these enlarged lysosomes using immunofluorescence staining with galectin-3, which binds to β-galactosides on the luminal glycoproteins of the ruptured membranes of endosomes or lysosomes [25]. In untreated cells, galectin-3 was distributed evenly in the cytoplasm. However, in TFP-treated melanoma cells, galectin-3 formed punctate structures in the enlarged lysosomes (**Figure 4B**). Taken together, the results indicated that TFP damaged lysosomal membranes, which led to LMP.

Lysosomal membrane permeabilization-induced cell death is STAT3 dependent in melanoma brain metastatic cells

Previous studies have shown that LMP which initiates a cascade of events leading to the degradation of vital cellular proteins/components can cause cell death [26, 27]. We thus used release of LDH as a measure of the cytotoxicity of TFP. Treatment of cells with TFP resulted in a significant increase in the release of LDH (**Figure 5A**). To test whether the cytotoxic ef-

fects of TFP were dependent on LMP, we combined TFP treatment with an inhibitor of cathepsin D, pepstatin A. LDH release decreased significantly in TFP-treated cells in the presence of pepstatin A (**Figure 5A**). These results suggested that TFP-induced cell death is LMP-dependent.

Recent studies have found that the transcription factor STAT3 might mediate LMP [28-30], through activation of the expression of cathepsins and suppression of the endogenous cathepsin inhibitor, Spi2A. Treatment with TFP increased the levels of phosphorylated STAT3, its active form, in melanoma brain metastatic cells in a dose-dependent manner (**Figure 5B**). The total protein levels of STAT3 were however not affected. To test whether the cell death caused by TFP is STAT3 dependent, we transfected H1 and Melmet 1 cell lines with siRNAs targeting STAT3 (Figure S6). H1- and Melmet 1-siSTAT3 cells had less damage to lysosomal membranes (highlighted with galectin-3) under TFP treatment compared to TFP treatment of the parental cell lines (**Figure 5C**). We also found that H1- and Melmet 1-siSTAT3 cells released significantly less LDH after TFP treatment relative to TFP treated parental cell lines (**Figure 5D**). In summary, our data suggest that TFP treatment causes LMP-induced cell death, which is STAT3 dependent.

Discussion

Melanoma has a tremendous propensity to metastasize to the brain. Despite aggressive treatment, the prognosis for patients with melanoma brain metastasis remains poor. A challenge even today with the current crop of targeted drugs is that most are still too large to penetrate the BBB. Recently, drug repurposing has gained increased attention in cancer treatment [31]. Repurposed drugs often have other mechanisms of action beyond the purpose for which they were developed, and therefore may be exploited for other maladies including cancer. These drugs often have documented safety profiles, after many years of clinical use. Drug repurposing also cuts through years of laborious and expensive drug development [32, 33]. In the current work, we show that the antipsychotic drug trifluoperazine (TFP) may be repurposed for the treatment of melanoma brain metastasis. Using a well-established animal model for melanoma brain metastasis, we found that TFP treatment decreased the brain metastatic tumor burden, and improved animal survival.

A characteristic essential for efficacy of drugs in the treatment of brain metastasis is the ability to penetrate an intact BBB [34]. Early in brain metastatic tumor progression, the brain lesions are too small to destroy the BBB, and they are thus not visible on contrast enhanced MRI [8]. Due to its favorable size (407.5 Da), TFP is able to penetrate an intact BBB, as previously shown by us [20] and others [15, 35]. TFP may thus be an attractive adjuvant to current established therapies for melanoma brain metastasis.

Our work showed that TFP decreased cell viability, cell proliferation and spheroid growth. TFP caused lysosomal membrane permeabilization (LMP), which is characterized by decreased cytosolic but increased lysosomal pH, perturbed iron homeostasis, defects in lysosomal cytoprotective factors and release of hydrolases into the cytosol. More importantly, LMP is associated with cell death [26]. We found that TFP treatment also induced cell death, and furthermore the process appeared to be mediated by the transcription factor STAT3. Our results, that TFP causes LMP and cell death through STAT3, corroborate the work of previous studies [29].

STAT3 is a cell proliferation-related transcription factor that regulates numerous apoptosis-related proteins, including Bcl-2, Bcl-xL, Mcl-1, and cyclin D1. STAT3 is also reported to function as an oncogene in tumorigenesis and tumor development [36]. Recently, several studies have reported that STAT3 controls the process of LMP, which leads to cell death [28-30]. The underlying mechanism may be that STAT3 at least partially inhibits the transcriptional activity of transcription factor EB (TFEB), which is involved in lysosome biogenesis [37]. STAT3 thus renders TFEB unable to facilitate lysosomal repair and biogenesis, subsequently contributing to further lysosomal instability and cell death [30]. These studies also suggest that STAT3 could have other, yet unidentified roles, in addition to being oncogenic. However, we have not investigated whether STAT3 has an oncogenic role in our brain metastasis model.

In summary, TFP showed efficient anti-tumor effects and increased survival in an experimental brain metastasis model. STAT3 and LMP mediate the response of cells to TFP. Our data should therefore encourage further investigation into the efficacy of TFP as an adjuvant therapy for the treatment of melanoma brain metastases in the clinical setting.

In this study we report for the first time that TFP inhibited the growth of melanoma brain metastases and prolonged animal survival after injection of tumor cells. On the molecular level, TFP was cytotoxic to melanoma brain metastases based on TFP-induced lysosomal membrane permeabilization and cell death appeared to be STAT3 dependent. Our study provided more basis for further clinical investigation of TFP as an efficient therapy for patients with brain metastases.

Acknowledgements

This work was supported by the Western Norway Regional Health Authority, Stiftelsen Kristian Gerhard Jebsen, the University of Bergen, the Norwegian Cancer Society, the Norwegian Research Council, the National Natural Science Foundation of China (81702474, 81972351, 81903126), the Department of Science & Technology of Shandong Province (2017CXGC1502 and 2018GSF118082), the Special Foundation for Taishan Scholars (ts-20110814 and tshw201502056), the Shandong Provincial Natural Science Foundation (ZR2017MH116), the China Postdoctoral Science Foundation (2018M642666), and the Jinan Science and Technology Bureau of Shandong Province (201704096).

Disclosure of conflict of interest

None.

Abbreviations

AO, acridine orange; BBB, blood-brain-barrier; GBM, glioblastoma; GFP, green fluorescent protein; H&E, Hematoxylin and Eosin; LDH, Lactate dehydrogenase; LMP, lysosomal membrane permeabilization; MRI, Magnetic resonance imaging; RFP, red fluorescent protein; TEM, Transmission electron microscopy; TFEB, transcription factor EB; TFP, trifluoperazine; WBRT, whole-brain radiotherapy.

Address correspondence to: Dr. Frits Thorsen, Kristian Gerhard Jebsen Brain Tumour Research Centre, Department of Biomedicine, University of Bergen, Bergen, Norway; Molecular Imaging Center, University of Bergen, Bergen, Norway. E-mail: Frits.Thorsen@uib.no; Drs. Xingang Li and Jian Wang, Department of Neurosurgery, Qilu Hospital of Shandong University and Brain Science Research Institute, Shandong University, Jinan, China; Shandong Key Laboratory of Brain Function Remodeling, China. E-mail: lixg@sdu.edu.cn (XGL); jian.wang@uib.no (JW)

References

[1] Vosoughi E, Lee JM, Miller JR, Nosrati M, Minor DR, Abendroth R, Lee JW, Andrews BT, Leng LZ, Wu M, Leong SP, Kashani-Sabet M and Kim KB. Survival and clinical outcomes of patients with melanoma brain metastasis in the era of checkpoint inhibitors and targeted therapies. BMC Cancer 2018; 18: 490.

[2] Tosoni A, Ermani M and Brandes AA. The pathogenesis and treatment of brain metastases: a comprehensive review. Crit Rev Oncol Hematol 2004; 52: 199-215.

[3] Fonkem E, Uhlmann EJ, Floyd SR, Mahadevan A, Kasper E, Eton O and Wong ET. Melanoma brain metastasis: overview of current management and emerging targeted therapies. Expert Rev Neurother 2012; 12: 1207-15.

[4] Tawbi HA, Forsyth PA, Algazi A, Hamid O, Hodi FS, Moschos SJ, Khushalani NI, Lewis K, Lao CD, Postow MA, Atkins MB, Ernstoff MS, Reardon DA, Puzanov I, Kudchadkar RR, Thomas RP, Tarhini A, Pavlick AC, Jiang J, Avila A, Demelo S and Margolin K. Combined nivolumab and ipilimumab in melanoma metastatic to the brain. N Engl J Med 2018; 379: 722-730.

[5] Hannan EJ, O'Leary DP, MacNally SP, Kay EW, Farrell MA, Morris PG, Power CP and Hill ADK. The significance of BRAF V600E mutation status discordance between primary cutaneous melanoma and brain metastases: the implications for BRAF inhibitor therapy. Medicine (Baltimore) 2017; 96: e8404.

[6] Davies MA, Saiag P, Robert C, Grob JJ, Flaherty KT, Arance A, Chiarion-Sileni V, Thomas L, Lesimple T, Mortier L, Moschos SJ, Hogg D, Márquez-Rodas I, Del Vecchio M, Lebbé C15, Meyer N, Zhang Y, Huang Y, Mookerjee B and Long GV. Dabrafenib plus trametinib in patients with BRAF(V600)-mutant melanoma brain metastases (COMBI-MB): a multicentre, multicohort, open-label, phase 2 trial. Lancet Oncol 2017; 18: 863-873.

[7] Liu X, Wu J, Qin H and Xu J. The role of autophagy in the resistance to BRAF inhibition in

BRAF-mutated melanoma. Target Oncol 2018; 13: 437-446.

[8] Thorsen F, Fite B, Mahakian LM, Seo JW, Qin S, Harrison V, Johnson S, Ingham E, Caskey C, Sundstrøm T, Meade TJ, Harter PN, Skaftnesmo KO and Ferrara KW. Multimodal imaging enables early detection and characterization of changes in tumor permeability of brain metastases. J Control Release 2013; 172: 812-22.

[9] Klionsky DJ, Abdelmohsen K, Abe A, Abedin MJ, Abeliovich H, Acevedo Arozena A, Adachi H, Adams CM, Adams PD, Adeli K, Adhihetty PJ, Adler SG, Agam G, Agarwal R, Aghi MK, Agnello M, Agostinis P, Aguilar PV, Aguirre-Ghiso J, Airoldi EM, Ait-Si-Ali S, Akematsu T, Akporiaye ET, Al-Rubeai M, Albaiceta GM, Albanese C, Albani D, Albert ML, Aldudo J, Algül H, Alirezaei M, Alloza I, Almasan A, Almonte-Beceril M, Alnemri ES, Alonso C, Altan-Bonnet N, Altieri DC, Alvarez S, Alvarez-Erviti L, Alves S, Amadoro G, Amano A, Amantini C, Ambrosio S, Amelio I, Amer AO, Amessou M, Amon A, An Z, Anania FA, Andersen SU, Andley UP, Andreadi CK, Andrieu-Abadie N, Anel A, Ann DK, Anoopkumar-Dukie S, Antonioli M, Aoki H, Apostolova N, Aquila S, Aquilano K, Araki K, Arama E, Aranda A, Araya J, Arcaro A, Arias E, Arimoto H, Ariosa AR, Armstrong JL, Arnould T, Arsov I, Asanuma K, Askanas V, Asselin E, Atarashi R, Atherton SS, Atkin JD, Attardi LD, Auberger P, Auburger G, Aurelian L, Autelli R, Avagliano L, Avantaggiati ML, Avrahami L, Awale S, Azad N, Bachetti T, Backer JM, Bae DH, Bae JS, Bae ON, Bae SH, Baehrecke EH, Baek SH, Baghdiguian S, Bagniewska-Zadworna A, Bai H, Bai J, Bai XY, Bailly Y, Balaji KN, Balduini W, Ballabio A, Balzan R, Banerjee R, Bánhegyi G, Bao H, Barbeau B, Barrachina MD, Barreiro E, Bartel B, Bartolomé A, Bassham DC, Bassi MT, Bast RC Jr, Basu A, Batista MT, Batoko H, Battino M, Bauckman K, Baumgarner BL, Bayer KU, Beale R, Beaulieu JF, Beck GR Jr, Becker C, Beckham JD, Bédard PA, Bednarski PJ, Begley TJ, Behl C, Behrends C, Behrens GM, Behrns KE, Bejarano E, Belaid A, Belleudi F, Bénard G, Berchem G, Bergamaschi D, Bergami M, Berkhout B, Berliocchi L, Bernard A, Bernard M, Bernassola F, Bertolotti A, Bess AS, Besteiro S, Bettuzzi S, Bhalla S, Bhattacharyya S, Bhutia SK, Biagosch C, Bianchi MW, Biard-Piechaczyk M, Billes V, Bincoletto C, Bingol B, Bird SW, Bitoun M, Bjedov I, Blackstone C, Blanc L, Blanco GA, Blomhoff HK, Boada-Romero E, Böckler S, Boes M, Boesze-Battaglia K, Boise LH, Bolino A, Boman A, Bonaldo P, Bordi M, Bosch J, Botana LM, Botti J, Bou G, Bouché M, Bouchecareilh M, Boucher MJ, Boulton ME, Bouret SG, Boya P, Boyer-Guittaut M, Bozhkov PV, Brady N, Braga VM, Brancolini C, Braus GH, Bravo-San Pedro JM, Brennan LA, Bresnick EH, Brest P, Bridges D, Bringer MA, Brini M, Brito GC, Brodin B, Brookes PS, Brown EJ, Brown K, Broxmeyer HE, Bruhat A, Brum PC, Brumell JH, Brunetti-Pierri N, Bryson-Richardson RJ, Buch S, Buchan AM, Budak H, Bulavin DV, Bultman SJ, Bultynck G, Bumbasirevic V, Burelle Y, Burke RE, Burmeister M, Bütikofer P, Caberlotto L, Cadwell K, Cahova M, Cai D, Cai J, Cai Q, Calatayud S, Camougrand N, Campanella M, Campbell GR, Campbell M, Campello S, Candau R, Caniggia I, Cantoni L, Cao L, Caplan AB, Caraglia M, Cardinali C, Cardoso SM, Carew JS, Carleton LA, Carlin CR, Carloni S, Carlsson SR, Carmona-Gutierrez D, Carneiro LA, Carnevali O, Carra S, Carrier A, Carroll B, Casas C, Casas J, Cassinelli G, Castets P, Castro-Obregon S, Cavallini G, Ceccherini I, Cecconi F, Cederbaum AI, Ceña V, Cenci S, Cerella C, Cervia D, Cetrullo S, Chaachouay H, Chae HJ, Chagin AS, Chai CY, Chakrabarti G, Chamilos G, Chan EY, Chan MT, Chandra D, Chandra P, Chang CP, Chang RC, Chang TY, Chatham JC, Chatterjee S, Chauhan S, Che Y, Cheetham ME, Cheluvappa R, Chen CJ, Chen G, Chen GC, Chen G, Chen H, Chen JW, Chen JK, Chen M, Chen M, Chen P, Chen Q, Chen Q, Chen SD, Chen S, Chen SS, Chen W, Chen WJ, Chen WQ, Chen W, Chen X, Chen YH, Chen YG, Chen Y, Chen Y, Chen Y, Chen YJ, Chen YQ, Chen Y, Chen Z, Chen Z, Cheng A, Cheng CH, Cheng H, Cheong H, Cherry S, Chesney J, Cheung CH, Chevet E, Chi HC, Chi SG, Chiacchiera F, Chiang HL, Chiarelli R, Chiariello M, Chieppa M, Chin LS, Chiong M, Chiu GN, Cho DH, Cho SG, Cho WC, Cho YY, Cho YS, Choi AM, Choi EJ, Choi EK, Choi J, Choi ME, Choi SI, Chou TF, Chouaib S, Choubey D, Choubey V, Chow KC, Chowdhury K, Chu CT, Chuang TH, Chun T, Chung H, Chung T, Chung YL, Chwae YJ, Cianfanelli V, Ciarcia R, Ciechomska IA, Ciriolo MR, Cirone M, Claerhout S, Clague MJ, Clària J, Clarke PG, Clarke R, Clementi E, Cleyrat C, Cnop M, Coccia EM, Cocco T, Codogno P, Coers J, Cohen EE, Colecchia D, Coletto L, Coll NS, Colucci-Guyon E, Comincini S, Condello M, Cook KL, Coombs GH, Cooper CD, Cooper JM, Coppens I, Corasaniti MT, Corazzari M, Corbalan R, Corcelle-Termeau E, Cordero MD, Corral-Ramos C, Corti O, Cossarizza A, Costelli P, Costes S, Cotman SL, Coto-Montes A, Cottet S, Couve E, Covey LR, Cowart LA, Cox JS, Coxon FP, Coyne CB, Cragg MS, Craven RJ, Crepaldi T, Crespo JL, Criollo A, Crippa V, Cruz MT, Cuervo AM, Cuezva JM, Cui T, Cutillas PR, Czaja MJ, Czyzyk-Krzeska MF, Dagda RK, Dahmen U, Dai C, Dai W, Dai Y, Dalby KN, Dalla Valle L, Dalmasso G, D'Amelio M, Damme M, Darfeuille-Michaud A,

Dargemont C, Darley-Usmar VM, Dasarathy S, Dasgupta B, Dash S, Dass CR, Davey HM, Davids LM, Dávila D, Davis RJ, Dawson TM, Dawson VL, Daza P, de Belleroche J, de Figueiredo P, de Figueiredo RC, de la Fuente J, De Martino L, De Matteis A, De Meyer GR, De Milito A, De Santi M, de Souza W, De Tata V, De Zio D, Debnath J, Dechant R, Decuypere JP, Deegan S, Dehay B, Del Bello B, Del Re DP, Delage-Mourroux R, Delbridge LM, Deldicque L, Delorme-Axford E, Deng Y, Dengjel J, Denizot M, Dent P, Der CJ, Deretic V, Derrien B, Deutsch E, Devarenne TP, Devenish RJ, Di Bartolomeo S, Di Daniele N, Di Domenico F, Di Nardo A, Di Paola S, Di Pietro A, Di Renzo L, DiAntonio A, Díaz-Araya G, Díaz-Laviada I, Diaz-Meco MT, Diaz-Nido J, Dickey CA, Dickson RC, Diederich M, Digard P, Dikic I, Dinesh-Kumar SP, Ding C, Ding WX, Ding Z, Dini L, Distler JH, Diwan A, Djavaheri-Mergny M, Dmytruk K, Dobson RC, Doetsch V, Dokladny K, Dokudovskaya S, Donadelli M, Dong XC, Dong X, Dong Z, Donohue TM Jr, Doran KS, D'Orazi G, Dorn GW 2nd, Dosenko V, Dridi S, Drucker L, Du J, Du LL, Du L, du Toit A, Dua P, Duan L, Duann P, Dubey VK, Duchen MR, Duchosal MA, Duez H, Dugail I, Dumit VI, Duncan MC, Dunlop EA, Dunn WA Jr, Dupont N, Dupuis L, Durán RV, Durcan TM, Duvezin-Caubet S, Duvvuri U, Eapen V, Ebrahimi-Fakhari D, Echard A, Eckhart L, Edelstein CL, Edinger AL, Eichinger L, Eisenberg T, Eisenberg-Lerner A, Eissa NT, El-Deiry WS, El-Khoury V, Elazar Z, Eldar-Finkelman H, Elliott CJ, Emanuele E, Emmenegger U, Engedal N, Engelbrecht AM, Engelender S, Enserink JM, Erdmann R, Erenpreisa J, Eri R, Eriksen JL, Erman A, Escalante R, Eskelinen EL, Espert L, Esteban-Martínez L, Evans TJ, Fabri M, Fabrias G, Fabrizi C, Facchiano A, Færgeman NJ, Faggioni A, Fairlie WD, Fan C, Fan D, Fan J, Fang S, Fanto M, Fanzani A, Farkas T, Faure M, Favier FB, Fearnhead H, Federici M, Fei E, Felizardo TC, Feng H, Feng Y, Feng Y, Ferguson TA, Fernández ÁF, Fernandez-Barrena MG, Fernandez-Checa JC, Fernández-López A, Fernandez-Zapico ME, Feron O, Ferraro E, Ferreira-Halder CV, Fesus L, Feuer R, Fiesel FC, Filippi-Chiela EC, Filomeni G, Fimia GM, Fingert JH, Finkbeiner S, Finkel T, Fiorito F, Fisher PB, Flajolet M, Flamigni F, Florey O, Florio S, Floto RA, Folini M, Follo C, Fon EA, Fornai F, Fortunato F, Fraldi A, Franco R, Francois A, François A, Frankel LB, Fraser ID, Frey N, Freyssenet DG, Frezza C, Friedman SL, Frigo DE, Fu D, Fuentes JM, Fueyo J, Fujitani Y, Fujiwara Y, Fujiya M, Fukuda M, Fulda S, Fusco C, Gabryel B, Gaestel M, Gailly P, Gajewska M, Galadari S, Galili G, Galindo I, Galindo MF, Galliciotti G, Galluzzi L, Galluzzi L, Galy V, Gammoh N, Gandy S, Ganesan AK, Ganesan S, Ganley IG, Gannagé M, Gao FB, Gao F, Gao JX, García Nannig L, García Véscovi E, Garcia-Macía M, Garcia-Ruiz C, Garg AD, Garg PK, Gargini R, Gassen NC, Gatica D, Gatti E, Gavard J, Gavathiotis E, Ge L, Ge P, Ge S, Gean PW, Gelmetti V, Genazzani AA, Geng J, Genschik P, Gerner L, Gestwicki JE, Gewirtz DA, Ghavami S, Ghigo E, Ghosh D, Giammarioli AM, Giampieri F, Giampietri C, Giatromanolaki A, Gibbings DJ, Gibellini L, Gibson SB, Ginet V, Giordano A, Giorgini F, Giovannetti E, Girardin SE, Gispert S, Giuliano S, Gladson CL, Glavic A, Gleave M, Godefroy N, Gogal RM Jr, Gokulan K, Goldman GH, Goletti D, Goligorsky MS, Gomes AV, Gomes LC, Gomez H, Gomez-Manzano C, Gómez-Sánchez R, Gonçalves DA, Goncu E, Gong Q, Gongora C, Gonzalez CB, Gonzalez-Alegre P, Gonzalez-Cabo P, González-Polo RA, Goping IS, Gorbea C, Gorbunov NV, Goring DR, Gorman AM, Gorski SM, Goruppi S, Goto-Yamada S, Gotor C, Gottlieb RA, Gozes I, Gozuacik D, Graba Y, Graef M, Granato GE, Grant GD, Grant S, Gravina GL, Green DR, Greenhough A, Greenwood MT, Grimaldi B, Gros F, Grose C, Groulx JF, Gruber F, Grumati P, Grune T, Guan JL, Guan KL, Guerra B, Guillen C, Gulshan K, Gunst J, Guo C, Guo L, Guo M, Guo W, Guo XG, Gust AA, Gustafsson ÅB, Gutierrez E, Gutierrez MG, Gwak HS, Haas A, Haber JE, Hadano S, Hagedorn M, Hahn DR, Halayko AJ, Hamacher-Brady A, Hamada K, Hamai A, Hamann A, Hamasaki M, Hamer I, Hamid Q, Hammond EM, Han F, Han W, Handa JT, Hanover JA, Hansen M, Harada M, Harhaji-Trajkovic L, Harper JW, Harrath AH, Harris AL, Harris J, Hasler U, Hasselblatt P, Hasui K, Hawley RG, Hawley TS, He C, He CY, He F, He G, He RR, He XH, He YW, He YY, Heath JK, Hébert MJ, Heinzen RA, Helgason GV, Hensel M, Henske EP, Her C, Herman PK, Hernández A, Hernandez C, Hernández-Tiedra S, Hetz C, Hiesinger PR, Higaki K, Hilfiker S, Hill BG, Hill JA, Hill WD, Hino K, Hofius D, Hofman P, Höglinger GU, Höhfeld J, Holz MK, Hong Y, Hood DA, Hoozemans JJ, Hoppe T, Hsu C, Hsu CY, Hsu LC, Hu D, Hu G, Hu HM, Hu H, Hu MC, Hu YC, Hu ZW, Hua F, Hua Y, Huang C, Huang HL, Huang KH, Huang KY, Huang S, Huang S, Huang WP, Huang YR, Huang Y, Huang Y, Huber TB, Huebbe P, Huh WK, Hulmi JJ, Hur GM, Hurley JH, Husak Z, Hussain SN, Hussain S, Hwang JJ, Hwang S, Hwang TI, Ichihara A, Imai Y, Imbriano C, Inomata M, Into T, Iovane V, Iovanna JL, Iozzo RV, Ip NY, Irazoqui JE, Iribarren P, Isaka Y, Isakovic AJ, Ischiropoulos H, Isenberg JS, Ishaq M, Ishida H, Ishii I, Ishmael JE, Isidoro C, Isobe K, Isono E, Issazadeh-Navikas S, Itahana K, Itakura E, Ivanov AI, Iyer AK, Izquierdo JM, Izumi Y, Izzo V, Jäättelä M, Jaber N, Jackson DJ, Jackson WT, Jacob TG, Jacques TS, Jagannath

C, Jain A, Jana NR, Jang BK, Jani A, Janji B, Jannig PR, Jansson PJ, Jean S, Jendrach M, Jeon JH, Jessen N, Jeung EB, Jia K, Jia L, Jiang H, Jiang H, Jiang L, Jiang T, Jiang X, Jiang X, Jiang X, Jiang Y, Jiang Y, Jiménez A, Jin C, Jin H, Jin L, Jin M, Jin S, Jinwal UK, Jo EK, Johansen T, Johnson DE, Johnson GV, Johnson JD, Jonasch E, Jones C, Joosten LA, Jordan J, Joseph AM, Joseph B, Joubert AM, Ju D, Ju J, Juan HF, Juenemann K, Juhász G, Jung HS, Jung JU, Jung YK, Jungbluth H, Justice MJ, Jutten B, Kaakoush NO, Kaarniranta K, Kaasik A, Kabuta T, Kaeffer B, Kågedal K, Kahana A, Kajimura S, Kakhlon O, Kalia M, Kalvakolanu DV, Kamada Y, Kambas K, Kaminskyy VO, Kampinga HH, Kandouz M, Kang C, Kang R, Kang TC, Kanki T, Kanneganti TD, Kanno H, Kanthasamy AG, Kantorow M, Kaparakis-Liaskos M, Kapuy O, Karantza V, Karim MR, Karmakar P, Kaser A, Kaushik S, Kawula T, Kaynar AM, Ke PY, Ke ZJ, Kehrl JH, Keller KE, Kemper JK, Kenworthy AK, Kepp O, Kern A, Kesari S, Kessel D, Ketteler R, Kettelhut Ido C, Khambu B, Khan MM, Khandelwal VK, Khare S, Kiang JG, Kiger AA, Kihara A, Kim AL, Kim CH, Kim DR, Kim DH, Kim EK, Kim HY, Kim HR, Kim JS, Kim JH, Kim JC, Kim JH, Kim KW, Kim MD, Kim MM, Kim PK, Kim SW, Kim SY, Kim YS, Kim Y, Kimchi A, Kimmelman AC, Kimura T, King JS, Kirkegaard K, Kirkin V, Kirshenbaum LA, Kishi S, Kitajima Y, Kitamoto K, Kitaoka Y, Kitazato K, Kley RA, Klimecki WT, Klinkenberg M, Klucken J, Knævelsrud H, Knecht E, Knuppertz L, Ko JL, Kobayashi S, Koch JC, Koechlin-Ramonatxo C, Koenig U, Koh YH, Köhler K, Kohlwein SD, Koike M, Komatsu M, Kominami E, Kong D, Kong HJ, Konstantakou EG, Kopp BT, Korcsmaros T, Korhonen L, Korolchuk VI, Koshkina NV, Kou Y, Koukourakis MI, Koumenis C, Kovács AL, Kovács T, Kovacs WJ, Koya D, Kraft C, Krainc D, Kramer H, Kravic-Stevovic T, Krek W, Kretz-Remy C, Krick R, Krishnamurthy M, Kriston-Vizi J, Kroemer G, Kruer MC, Kruger R, Ktistakis NT, Kuchitsu K, Kuhn C, Kumar AP, Kumar A, Kumar A, Kumar D, Kumar D, Kumar R, Kumar S, Kundu M, Kung HJ, Kuno A, Kuo SH, Kuret J, Kurz T, Kwok T, Kwon TK, Kwon YT, Kyrmizi I, La Spada AR, Lafont F, Lahm T, Lakkaraju A, Lam T, Lamark T, Lancel S, Landowski TH, Lane DJ, Lane JD, Lanzi C, Lapaquette P, Lapierre LR, Laporte J, Laukkarinen J, Laurie GW, Lavandero S, Lavie L, LaVoie MJ, Law BY, Law HK, Law KB, Layfield R, Lazo PA, Le Cam L, Le Roch KG, Le Stunff H, Leardkamolkarn V, Lecuit M, Lee BH, Lee CH, Lee EF, Lee GM, Lee HJ, Lee H, Lee JK, Lee J, Lee JH, Lee JH, Lee M, Lee MS, Lee PJ, Lee SW, Lee SJ, Lee SJ, Lee SY, Lee SH, Lee SS, Lee SJ, Lee S, Lee YR, Lee YJ, Lee YH, Leeuwenburgh C, Lefort S, Legouis R, Lei J, Lei QY, Leib DA, Leibowitz G, Lekli I, Lemaire SD, Lemasters JJ, Lemberg MK, Lemoine A, Leng S, Lenz G, Lenzi P, Lerman LO, Lettieri Barbato D, Leu JI, Leung HY, Levine B, Lewis PA, Lezoualc'h F, Li C, Li F, Li FJ, Li J, Li K, Li L, Li M, Li M, Li Q, Li R, Li S, Li W, Li W, Li X, Li Y, Lian J, Liang C, Liang Q, Liao Y, Liberal J, Liberski PP, Lie P, Lieberman AP, Lim HJ, Lim KL, Lim K, Lima RT, Lin CS, Lin CF, Lin F, Lin F, Lin FC, Lin K, Lin KH, Lin PH, Lin T, Lin WW, Lin YS, Lin Y, Linden R, Lindholm D, Lindqvist LM, Lingor P, Linkermann A, Liotta LA, Lipinski MM, Lira VA, Lisanti MP, Liton PB, Liu B, Liu C, Liu CF, Liu F, Liu HJ, Liu J, Liu JJ, Liu JL, Liu K, Liu L, Liu L, Liu Q, Liu RY, Liu S, Liu S, Liu W, Liu XD, Liu X, Liu XH, Liu X, Liu X, Liu X, Liu Y, Liu Y, Liu Z, Liu Z, Liuzzi JP, Lizard G, Ljujic M, Lodhi IJ, Logue SE, Lokeshwar BL, Long YC, Lonial S, Loos B, López-Otín C, López-Vicario C, Lorente M, Lorenzi PL, Lõrincz P, Los M, Lotze MT, Lovat PE, Lu B, Lu B, Lu J, Lu Q, Lu SM, Lu S, Lu Y, Luciano F, Luckhart S, Lucocq JM, Ludovico P, Lugea A, Lukacs NW, Lum JJ, Lund AH, Luo H, Luo J, Luo S, Luparello C, Lyons T, Ma J, Ma Y, Ma Y, Ma Z, Machado J, Machado-Santelli GM, Macian F, MacIntosh GC, MacKeigan JP, Macleod KF, MacMicking JD, MacMillan-Crow LA, Madeo F, Madesh M, Madrigal-Matute J, Maeda A, Maeda T, Maegawa G, Maellaro E, Maes H, Magariños M, Maiese K, Maiti TK, Maiuri L, Maiuri MC, Maki CG, Malli R, Malorni W, Maloyan A, Mami-Chouaib F, Man N, Mancias JD, Mandelkow EM, Mandell MA, Manfredi AA, Manié SN, Manzoni C, Mao K, Mao Z, Mao ZW, Marambaud P, Marconi AM, Marelja Z, Marfe G, Margeta M, Margittai E, Mari M, Mariani FV, Marin C, Marinelli S, Mariño G, Markovic I, Marquez R, Martelli AM, Martens S, Martin KR, Martin SJ, Martin S, Martin-Acebes MA, Martín-Sanz P, Martinand-Mari C, Martinet W, Martinez J, Martinez-Lopez N, Martinez-Outschoorn U, Martínez-Velázquez M, Martinez-Vicente M, Martins WK, Mashima H, Mastrianni JA, Matarese G, Matarrese P, Mateo R, Matoba S, Matsumoto N, Matsushita T, Matsuura A, Matsuzawa T, Mattson MP, Matus S, Maugeri N, Mauvezin C, Mayer A, Maysinger D, Mazzolini GD, McBrayer MK, McCall K, McCormick C, McInerney GM, McIver SC, McKenna S, McMahon JJ, McNeish IA, Mechta-Grigoriou F, Medema JP, Medina DL, Megyeri K, Mehrpour M, Mehta JL, Mei Y, Meier UC, Meijer AJ, Meléndez A, Melino G, Melino S, de Melo EJ, Mena MA, Meneghini MD, Menendez JA, Menezes R, Meng L, Meng LH, Meng S, Menghini R, Menko AS, Menna-Barreto RF, Menon MB, Meraz-Ríos MA, Merla G, Merlini L, Merlot AM, Meryk A, Meschini S, Meyer JN, Mi MT, Miao CY, Micale L, Michaeli S, Michiels C, Migliaccio AR, Miha-

ilidou AS, Mijaljica D, Mikoshiba K, Milan E, Miller-Fleming L, Mills GB, Mills IG, Minakaki G, Minassian BA, Ming XF, Minibayeva F, Minina EA, Mintern JD, Minucci S, Miranda-Vizuete A, Mitchell CH, Miyamoto S, Miyazawa K, Mizushima N, Mnich K, Mograbi B, Mohseni S, Moita LF, Molinari M, Molinari M, Møller AB, Mollereau B, Mollinedo F, Mongillo M, Monick MM, Montagnaro S, Montell C, Moore DJ, Moore MN, Mora-Rodriguez R, Moreira PI, Morel E, Morelli MB, Moreno S, Morgan MJ, Moris A, Moriyasu Y, Morrison JL, Morrison LA, Morselli E, Moscat J, Moseley PL, Mostowy S, Motori E, Mottet D, Mottram JC, Moussa CE, Mpakou VE, Mukhtar H, Mulcahy Levy JM, Muller S, Muñoz-Moreno R, Muñoz-Pinedo C, Münz C, Murphy ME, Murray JT, Murthy A, Mysorekar IU, Nabi IR, Nabissi M, Nader GA, Nagahara Y, Nagai Y, Nagata K, Nagelkerke A, Nagy P, Naidu SR, Nair S, Nakano H, Nakatogawa H, Nanjundan M, Napolitano G, Naqvi NI, Nardacci R, Narendra DP, Narita M, Nascimbeni AC, Natarajan R, Navegantes LC, Nawrocki ST, Nazarko TY, Nazarko VY, Neill T, Neri LM, Netea MG, Netea-Maier RT, Neves BM, Ney PA, Nezis IP, Nguyen HT, Nguyen HP, Nicot AS, Nilsen H, Nilsson P, Nishimura M, Nishino I, Niso-Santano M, Niu H, Nixon RA, Njar VC, Noda T, Noegel AA, Nolte EM, Norberg E, Norga KK, Noureini SK, Notomi S, Notterpek L, Nowikovsky K, Nukina N, Nürnberger T, O'Donnell VB, O'Donovan T, O'Dwyer PJ, Oehme I, Oeste CL, Ogawa M, Ogretmen B, Ogura Y, Oh YJ, Ohmuraya M, Ohshima T, Ojha R, Okamoto K, Okazaki T, Oliver FJ, Ollinger K, Olsson S, Orban DP, Ordonez P, Orhon I, Orosz L, O'Rourke EJ, Orozco H, Ortega AL, Ortona E, Osellame LD, Oshima J, Oshima S, Osiewacz HD, Otomo T, Otsu K, Ou JH, Outeiro TF, Ouyang DY, Ouyang H, Overholtzer M, Ozbun MA, Ozdinler PH, Ozpolat B, Pacelli C, Paganetti P, Page G, Pages G, Pagnini U, Pajak B, Pak SC, Pakos-Zebrucka K, Pakpour N, Palková Z, Palladino F, Pallauf K, Pallet N, Palmieri M, Paludan SR, Palumbo C, Palumbo S, Pampliega O, Pan H, Pan W, Panaretakis T, Pandey A, Pantazopoulou A, Papackova Z, Papademetrio DL, Papassideri I, Papini A, Parajuli N, Pardo J, Parekh VV, Parenti G, Park JI, Park J, Park OK, Parker R, Parlato R, Parys JB, Parzych KR, Pasquet JM, Pasquier B, Pasumarthi KB, Patschan D, Patterson C, Pattingre S, Pattison S, Pause A, Pavenstädt H, Pavone F, Pedrozo Z, Peña FJ, Peñalva MA, Pende M, Peng J, Penna F, Penninger JM, Pensalfini A, Pepe S, Pereira GJ, Pereira PC, Pérez-de la Cruz V, Pérez-Pérez ME, Pérez-Rodríguez D, Pérez-Sala D, Perier C, Perl A, Perlmutter DH, Perrotta I, Pervaiz S, Pesonen M, Pessin JE, Peters GJ, Petersen M, Petrache I, Petrof BJ, Petrovski G, Phang JM, Piacentini M, Pierdominici M, Pierre P, Pierrefite-Carle V, Pietrocola F, Pimentel-Muiños FX, Pinar M, Pineda B, Pinkas-Kramarski R, Pinti M, Pinton P, Piperdi B, Piret JM, Platanias LC, Platta HW, Plowey ED, Pöggeler S, Poirot M, Polčic P, Poletti A, Poon AH, Popelka H, Popova B, Poprawa I, Poulose SM, Poulton J, Powers SK, Powers T, Pozuelo-Rubio M, Prak K, Prange R, Prescott M, Priault M, Prince S, Proia RL, Proikas-Cezanne T, Prokisch H, Promponas VJ, Przyklenk K, Puertollano R, Pugazhenthi S, Puglielli L, Pujol A, Puyal J, Pyeon D, Qi X, Qian WB, Qin ZH, Qiu Y, Qu Z, Quadrilatero J, Quinn F, Raben N, Rabinowich H, Radogna F, Ragusa MJ, Rahmani M, Raina K, Ramanadham S, Ramesh R, Rami A, Randall-Demllo S, Randow F, Rao H, Rao VA, Rasmussen BB, Rasse TM, Ratovitski EA, Rautou PE, Ray SK, Razani B, Reed BH, Reggiori F, Rehm M, Reichert AS, Rein T, Reiner DJ, Reits E, Ren J, Ren X, Renna M, Reusch JE, Revuelta JL, Reyes L, Rezaie AR, Richards RI, Richardson DR, Richetta C, Riehle MA, Rihn BH, Rikihisa Y, Riley BE, Rimbach G, Rippo MR, Ritis K, Rizzi F, Rizzo E, Roach PJ, Robbins J, Roberge M, Roca G, Roccheri MC, Rocha S, Rodrigues CM, Rodríguez CI, de Cordoba SR, Rodriguez-Muela N, Roelofs J, Rogov VV, Rohn TT, Rohrer B, Romanelli D, Romani L, Romano PS, Roncero MI, Rosa JL, Rosello A, Rosen KV, Rosenstiel P, Rost-Roszkowska M, Roth KA, Roué G, Rouis M, Rouschop KM, Ruan DT, Ruano D, Rubinsztein DC, Rucker EB 3rd, Rudich A, Rudolf E, Rudolf R, Ruegg MA, Ruiz-Roldan C, Ruparelia AA, Rusmini P, Russ DW, Russo GL, Russo G, Russo R, Rusten TE, Ryabovol V, Ryan KM, Ryter SW, Sabatini DM, Sacher M, Sachse C, Sack MN, Sadoshima J, Saftig P, Sagi-Eisenberg R, Sahni S, Saikumar P, Saito T, Saitoh T, Sakakura K, Sakoh-Nakatogawa M, Sakuraba Y, Salazar-Roa M, Salomoni P, Saluja AK, Salvaterra PM, Salvioli R, Samali A, Sanchez AM, Sánchez-Alcázar JA, Sanchez-Prieto R, Sandri M, Sanjuan MA, Santaguida S, Santambrogio L, Santoni G, Dos Santos CN, Saran S, Sardiello M, Sargent G, Sarkar P, Sarkar S, Sarrias MR, Sarwal MM, Sasakawa C, Sasaki M, Sass M, Sato K, Sato M, Satriano J, Savaraj N, Saveljeva S, Schaefer L, Schaible UE, Scharl M, Schatzl HM, Schekman R, Scheper W, Schiavi A, Schipper HM, Schmeisser H, Schmidt J, Schmitz I, Schneider BE, Schneider EM, Schneider JL, Schon EA, Schönenberger MJ, Schönthal AH, Schorderet DF, Schröder B, Schuck S, Schulze RJ, Schwarten M, Schwarz TL, Sciarretta S, Scotto K, Scovassi AI, Screaton RA, Screen M, Seca H, Sedej S, Segatori L, Segev N, Seglen PO, Seguí-Simarro JM, Segura-Aguilar J, Seki E, Sell C,

Seiliez I, Semenkovich CF, Semenza GL, Sen U, Serra AL, Serrano-Puebla A, Sesaki H, Setoguchi T, Settembre C, Shacka JJ, Shajahan-Haq AN, Shapiro IM, Sharma S, She H, Shen CK, Shen CC, Shen HM, Shen S, Shen W, Sheng R, Sheng X, Sheng ZH, Shepherd TG, Shi J, Shi Q, Shi Q, Shi Y, Shibutani S, Shibuya K, Shidoji Y, Shieh JJ, Shih CM, Shimada Y, Shimizu S, Shin DW, Shinohara ML, Shintani M, Shintani T, Shioi T, Shirabe K, Shiri-Sverdlov R, Shirihai O, Shore GC, Shu CW, Shukla D, Sibirny AA, Sica V, Sigurdson CJ, Sigurdsson EM, Sijwali PS, Sikorska B, Silveira WA, Silvente-Poirot S, Silverman GA, Simak J, Simmet T, Simon AK, Simon HU, Simone C, Simons M, Simonsen A, Singh R, Singh SV, Singh SK, Sinha D, Sinha S, Sinicrope FA, Sirko A, Sirohi K, Sishi BJ, Sittler A, Siu PM, Sivridis E, Skwarska A, Slack R, Slaninová I, Slavov N, Smaili SS, Smalley KS, Smith DR, Soenen SJ, Soleimanpour SA, Solhaug A, Somasundaram K, Son JH, Sonawane A, Song C, Song F, Song HK, Song JX, Song W, Soo KY, Sood AK, Soong TW, Soontornniyomkij V, Sorice M, Sotgia F, Soto-Pantoja DR, Sotthibundhu A, Sousa MJ, Spaink HP, Span PN, Spang A, Sparks JD, Speck PG, Spector SA, Spies CD, Springer W, Clair DS, Stacchiotti A, Staels B, Stang MT, Starczynowski DT, Starokadomskyy P, Steegborn C, Steele JW, Stefanis L, Steffan J, Stellrecht CM, Stenmark H, Stepkowski TM, Stern ST, Stevens C, Stockwell BR, Stoka V, Storchova Z, Stork B, Stratoulias V, Stravopodis DJ, Strnad P, Strohecker AM, Ström AL, Stromhaug P, Stulik J, Su YX, Su Z, Subauste CS, Subramaniam S, Sue CM, Suh SW, Sui X, Sukseree S, Sulzer D, Sun FL, Sun J, Sun J, Sun SY, Sun Y, Sun Y, Sun Y, Sundaramoorthy V, Sung J, Suzuki H, Suzuki K, Suzuki N, Suzuki T, Suzuki YJ, Swanson MS, Swanton C, Swärd K, Swarup G, Sweeney ST, Sylvester PW, Szatmari Z, Szegezdi E, Szlosarek PW, Taegtmeyer H, Tafani M, Taillebourg E, Tait SW, Takacs-Vellai K, Takahashi Y, Takáts S, Takemura G, Takigawa N, Talbot NJ, Tamagno E, Tamburini J, Tan CP, Tan L, Tan ML, Tan M, Tan YJ, Tanaka K, Tanaka M, Tang D, Tang D, Tang G, Tanida I, Tanji K, Tannous BA, Tapia JA, Tasset-Cuevas I, Tatar M, Tavassoly I, Tavernarakis N, Taylor A, Taylor GS, Taylor GA, Taylor JP, Taylor MJ, Tchetina EV, Tee AR, Teixeira-Clerc F, Telang S, Tencomnao T, Teng BB, Teng RJ, Terro F, Tettamanti G, Theiss AL, Theron AE, Thomas KJ, Thomé MP, Thomes PG, Thorburn A, Thorner J, Thum T, Thumm M, Thurston TL, Tian L, Till A, Ting JP, Titorenko VI, Toker L, Toldo S, Tooze SA, Topisirovic I, Torgersen ML, Torosantucci L, Torriglia A, Torrisi MR, Tournier C, Towns R, Trajkovic V, Travassos LH, Triola G, Tripathi DN, Trisciuoglio D, Troncoso R, Trougakos IP, Truttmann AC, Tsai KJ, Tschan MP, Tseng YH, Tsukuba T, Tsung A, Tsvetkov AS, Tu S, Tuan HY, Tucci M, Tumbarello DA, Turk B, Turk V, Turner RF, Tveita AA, Tyagi SC, Ubukata M, Uchiyama Y, Udelnow A, Ueno T, Umekawa M, Umemiya-Shirafuji R, Underwood BR, Ungermann C, Ureshino RP, Ushioda R, Uversky VN, Uzcátegui NL, Vaccari T, Vaccaro MI, Váchová L, Vakifahmetoglu-Norberg H, Valdor R, Valente EM, Vallette F, Valverde AM, Van den Berghe G, Van Den Bosch L, van den Brink GR, van der Goot FG, van der Klei IJ, van der Laan LJ, van Doorn WG, van Egmond M, van Golen KL, Van Kaer L, van Lookeren Campagne M, Vandenabeele P, Vandenberghe W, Vanhorebeek I, Varela-Nieto I, Vasconcelos MH, Vasko R, Vavvas DG, Vega-Naredo I, Velasco G, Velentzas AD, Velentzas PD, Vellai T, Vellenga E, Vendelbo MH, Venkatachalam K, Ventura N, Ventura S, Veras PS, Verdier M, Vertessy BG, Viale A, Vidal M, Vieira HL, Vierstra RD, Vigneswaran N, Vij N, Vila M, Villar M, Villar VH, Villarroya J, Vindis C, Viola G, Viscomi MT, Vitale G, Vogl DT, Voitsekhovskaja OV, von Haefen C, von Schwarzenberg K, Voth DE, Vouret-Craviari V, Vuori K, Vyas JM, Waeber C, Walker CL, Walker MJ, Walter J, Wan L, Wan X, Wang B, Wang C, Wang CY, Wang C, Wang C, Wang C, Wang D, Wang F, Wang F, Wang G, Wang HJ, Wang H, Wang HG, Wang H, Wang HD, Wang J, Wang J, Wang M, Wang MQ, Wang PY, Wang P, Wang RC, Wang S, Wang TF, Wang X, Wang XJ, Wang XW, Wang X, Wang X, Wang Y, Wang Y, Wang Y, Wang YJ, Wang Y, Wang Y, Wang YT, Wang Y, Wang ZN, Wappner P, Ward C, Ward DM, Warnes G, Watada H, Watanabe Y, Watase K, Weaver TE, Weekes CD, Wei J, Weide T, Weihl CC, Weindl G, Weis SN, Wen L, Wen X, Wen Y, Westermann B, Weyand CM, White AR, White E, Whitton JL, Whitworth AJ, Wiels J, Wild F, Wildenberg ME, Wileman T, Wilkinson DS, Wilkinson S, Willbold D, Williams C, Williams K, Williamson PR, Winklhofer KF, Witkin SS, Wohlgemuth SE, Wollert T, Wolvetang EJ, Wong E, Wong GW, Wong RW, Wong VK, Woodcock EA, Wright KL, Wu C, Wu D, Wu GS, Wu J, Wu J, Wu M, Wu M, Wu S, Wu WK, Wu Y, Wu Z, Xavier CP, Xavier RJ, Xia GX, Xia T, Xia W, Xia Y, Xiao H, Xiao J, Xiao S, Xiao W, Xie CM, Xie Z, Xie Z, Xilouri M, Xiong Y, Xu C, Xu C, Xu F, Xu H, Xu H, Xu J, Xu J, Xu J, Xu L, Xu X, Xu Y, Xu Y, Xu ZX, Xu Z, Xue Y, Yamada T, Yamamoto A, Yamanaka K, Yamashina S, Yamashiro S, Yan B, Yan B, Yan X, Yan Z, Yanagi Y, Yang DS, Yang JM, Yang L, Yang M, Yang PM, Yang P, Yang Q, Yang W, Yang WY, Yang X, Yang Y, Yang Y, Yang Z, Yang Z, Yao MC, Yao PJ, Yao X, Yao Z, Yao Z, Yasui LS, Ye M, Yedvobnick B, Yeganeh B, Yeh ES, Yeyati PL, Yi F, Yi L, Yin XM, Yip CK, Yoo YM, Yoo YH, Yoon SY, Yoshida K, Yoshimori T, Young

KH, Yu H, Yu JJ, Yu JT, Yu J, Yu L, Yu WH, Yu XF, Yu Z, Yuan J, Yuan ZM, Yue BY, Yue J, Yue Z, Zacks DN, Zacksenhaus E, Zaffaroni N, Zaglia T, Zakeri Z, Zecchini V, Zeng J, Zeng M, Zeng Q, Zervos AS, Zhang DD, Zhang F, Zhang G, Zhang GC, Zhang H, Zhang H, Zhang H, Zhang H, Zhang J, Zhang J, Zhang J, Zhang J, Zhang JP, Zhang L, Zhang L, Zhang L, Zhang L, Zhang MY, Zhang X, Zhang XD, Zhang Y, Zhang Y, Zhang Y, Zhang Y, Zhang Y, Zhao M, Zhao WL, Zhao X, Zhao YG, Zhao Y, Zhao Y, Zhao YX, Zhao Z, Zhao ZJ, Zheng D, Zheng XL, Zheng X, Zhivotovsky B, Zhong Q, Zhou GZ, Zhou G, Zhou H, Zhou SF, Zhou XJ, Zhu H, Zhu H, Zhu WG, Zhu W, Zhu XF, Zhu Y, Zhuang SM, Zhuang X, Ziparo E, Zois CE, Zoladek T, Zong WX, Zorzano A and Zughaier SM. Guidelines for the use and interpretation of assays for monitoring autophagy (3rd edition). Autophagy 2016; 12: 1-222.

[10] Appelqvist H, Wäster P, Kågedal K and Öllinger K. The lysosome: from waste bag to potential therapeutic target. J Mol Cell Biol 2013; 5: 214-26.

[11] Zhang X, Wang J, Li X and Wang D. Lysosomes contribute to radioresistance in cancer. Cancer Lett 2018; 439: 39-46.

[12] Boya P. Lysosomal function and dysfunction: mechanism and disease. Antioxid Redox Signal 2012; 17: 766-74.

[13] Lubke T, Lobel P and Sleat DE. Proteomics of the lysosome. Biochim Biophys Acta 2009; 1793: 625-35.

[14] Galluzzi L, Vitale I, Aaronson SA, Abrams JM, Adam D, Agostinis P, Alnemri ES, Altucci L, Amelio I, Andrews DW, Annicchiarico-Petruzzelli M, Antonov AV, Arama E, Baehrecke EH, Barlev NA, Bazan NG, Bernassola F, Bertrand MJM, Bianchi K, Blagosklonny MV, Blomgren K, Borner C, Boya P, Brenner C, Campanella M, Candi E, Carmona-Gutierrez D, Cecconi F, Chan FK, Chandel NS, Cheng EH, Chipuk JE, Cidlowski JA, Ciechanover A, Cohen GM, Conrad M, Cubillos-Ruiz JR, Czabotar PE, D'Angiolella V, Dawson TM, Dawson VL, De Laurenzi V, De Maria R, Debatin KM, DeBerardinis RJ, Deshmukh M, Di Daniele N, Di Virgilio F, Dixit VM, Dixon SJ, Duckett CS, Dynlacht BD, El-Deiry WS, Elrod JW, Fimia GM, Fulda S, García-Sáez AJ, Garg AD, Garrido C, Gavathiotis E, Golstein P, Gottlieb E, Green DR, Greene LA, Gronemeyer H, Gross A, Hajnoczky G, Hardwick JM, Harris IS, Hengartner MO, Hetz C, Ichijo H, Jäättelä M, Joseph B, Jost PJ, Juin PP, Kaiser WJ, Karin M, Kaufmann T, Kepp O, Kimchi A, Kitsis RN, Klionsky DJ, Knight RA, Kumar S, Lee SW, Lemasters JJ, Levine B, Linkermann A, Lipton SA, Lockshin RA, López-Otín C, Lowe SW, Luedde T, Lugli E, MacFarlane M, Madeo F, Malewicz M, Malorni W, Manic G, Marine JC, Martin SJ, Martinou JC, Medema JP, Mehlen P, Meier P, Melino S, Miao EA, Molkentin JD, Moll UM, Muñoz-Pinedo C, Nagata S, Nuñez G, Oberst A, Oren M, Overholtzer M, Pagano M, Panaretakis T, Pasparakis M, Penninger JM, Pereira DM, Pervaiz S, Peter ME, Piacentini M, Pinton P, Prehn JHM, Puthalakath H, Rabinovich GA, Rehm M, Rizzuto R, Rodrigues CMP, Rubinsztein DC, Rudel T, Ryan KM, Sayan E, Scorrano L, Shao F, Shi Y, Silke J, Simon HU, Sistigu A, Stockwell BR, Strasser A, Szabadkai G, Tait SWG, Tang D, Tavernarakis N, Thorburn A, Tsujimoto Y, Turk B, Vanden Berghe T, Vandenabeele P, Vander Heiden MG, Villunger A, Virgin HW, Vousden KH, Vucic D, Wagner EF, Walczak H, Wallach D, Wang Y, Wells JA, Wood W, Yuan J, Zakeri Z, Zhivotovsky B, Zitvogel L, Melino G, Kroemer G. Molecular mechanisms of cell death: recommendations of the nomenclature committee on Cell Death 2018. Cell Death Differ 2018; 25: 486-541.

[15] Feng Z, Xia Y, Gao T, Xu F, Lei Q, Peng C, Yang Y, Xue Q, Hu X, Wang Q, Wang R, Ran Z, Zeng Z, Yang N, Xie Z and Yu L. The antipsychotic agent trifluoperazine hydrochloride suppresses triple-negative breast cancer tumor growth and brain metastasis by inducing G0/G1 arrest and apoptosis. Cell Death Dis 2018; 9: 1006.

[16] Howland RH. Trifluoperazine: a sprightly old drug. J Psychosoc Nurs Ment Health Serv 2016; 54: 20-2.

[17] Yeh CT, Wu AT, Chang PM, Chen KY, Yang CN, Yang SC, Ho CC, Chen CC, Kuo YL, Lee PY, Liu YW, Yen CC, Hsiao M, Lu PJ, Lai JM, Wang LS, Wu CH, Chiou JF, Yang PC and Huang CY. Trifluoperazine, an antipsychotic agent, inhibits cancer stem cell growth and overcomes drug resistance of lung cancer. Am J Respir Crit Care Med 2012; 186: 1180-8.

[18] Shin SY, Choi BH, Kim JR, Kim JH and Lee YH. Suppression of P-glycoprotein expression by antipsychotics trifluoperazine in adriamycin-resistant L1210 mouse leukemia cells. Eur J Pharm Sci 2006; 28: 300-6.

[19] Brosius SN, Turk AN, Byer SJ, Longo JF, Kappes JC, Roth KA and Carroll SL. Combinatorial therapy with tamoxifen and trifluoperazine effectively inhibits malignant peripheral nerve sheath tumor growth by targeting complementary signaling cascades. J Neuropathol Exp Neurol 2014; 73: 1078-90.

[20] Zhang X, Xu R, Zhang C, Xu Y, Han M, Huang B, Chen A, Qiu C, Thorsen F, Prestegarden L, Bjerkvig R, Wang J and Li X. Trifluoperazine, a novel autophagy inhibitor, increases radiosensitivity in glioblastoma by impairing homologous recombination. J Exp Clin Cancer Res 2017; 36: 118.

[21] Wang J, Daphu I, Pedersen PH, Miletic H, Hovland R, Mørk S, Bjerkvig R, Tiron C, McCormack E, Micklem D, Lorens JB, Immervoll H and

Thorsen F. A novel brain metastases model developed in immunodeficient rats closely mimics the growth of metastatic brain tumours in patients. Neuropathol Appl Neurobiol 2011; 37: 189-205.

[22] Aasen SN, Pospisilova A, Eichler TW, Panek J, Hruby M, Stepanek P, Spriet E, Jirak D, Skaftnesmo KO and Thorsen F. A novel nanoprobe for multimodal imaging is effectively incorporated into human melanoma metastatic cell lines. Int J Mol Sci 2015; 16: 21658-80.

[23] Repnik U, Hafner Česen M and Turk B. Lysosomal membrane permeabilization in cell death: concepts and challenges. Mitochondrion 2014; 19: 49-57.

[24] Sundstrøm T, Daphu I, Wendelbo I, Hodneland E, Lundervold A, Immervoll H, Skaftnesmo KO, Babic M, Jendelova P, Sykova E, Lund-Johansen M, Bjerkvig R and Thorsen F. Automated tracking of nanoparticle-labeled melanoma cells improves the predictive power of a brain metastasis model. Cancer Res 2013; 73: 2445-56.

[25] Maejima I, Takahashi A, Omori H, Kimura T, Takabatake Y, Saitoh T, Yamamoto A, Hamasaki M, Noda T, Isaka Y and Yoshimori T. Autophagy sequesters damaged lysosomes to control lysosomal biogenesis and kidney injury. EMBO J 2013; 32: 2336-47.

[26] Boya P and Kroemer G. Lysosomal membrane permeabilization in cell death. Oncogene 2008; 27: 6434-51.

[27] Domagala A, Fidyt K, Bobrowicz M, Stachura J, Szczygiel K and Firczuk M. Typical and atypical inducers of lysosomal cell death: a promising anticancer strategy. Int J Mol Sci 2018; 19.

[28] Li Y, Zhang Y, Gan Q, Xu M, Ding X, Tang G, Liang J, Liu K, Liu X, Wang X, Guo L, Gao Z, Hao X and Yang C. Elegans-based screen identifies lysosome-damaging alkaloids that induce STAT3-dependent lysosomal cell death. Protein Cell 2018; 9: 1013-1026.

[29] Sargeant TJ, Lloyd-Lewis B, Resemann HK, Ramos-Montoya A, Skepper J and Watson CJ. Stat3 controls cell death during mammary gland involution by regulating uptake of milk fat globules and lysosomal membrane permeabilization. Nat Cell Biol 2014; 16: 1057-1068.

[30] Li L, Sun B, Gao Y, Niu H, Yuan H and Lou H. STAT3 contributes to lysosomal-mediated cell death in a novel derivative of riccardin D-treated breast cancer cells in association with TFEB. Biochem Pharmacol 2018; 150: 267-279.

[31] Strittmatter SM. Overcoming drug development bottlenecks with repurposing: old drugs learn new tricks. Nat Med 2014; 20: 590-1.

[32] Zhang L, Yu J, Pan H, Hu P, Hao Y, Cai W, Zhu H, Yu AD, Xie X, Ma D and Yuan J. Small molecule regulators of autophagy identified by an image-based high-throughput screen. Proc Natl Acad Sci U S A 2007; 104: 19023-8.

[33] Tsvetkov AS, Miller J, Arrasate M, Wong JS, Pleiss MA and Finkbeiner S. A small-molecule scaffold induces autophagy in primary neurons and protects against toxicity in a Huntington disease model. Proc Natl Acad Sci U S A 2010; 107: 16982-7.

[34] Banks WA. From blood-brain barrier to blood-brain interface: new opportunities for CNS drug delivery. Nat Rev Drug Discov 2016; 15: 275-92.

[35] Marques-Santos LF, Bernardo RR, de Paula EF and Rumjanek VM. Cyclosporin A and trifluoperazine, two resistance-modulating agents, increase ivermectin neurotoxicity in mice. Pharmacol Toxicol 1999; 84: 125-9.

[36] Yu H, Lee H, Herrmann A, Buettner R and Jove R. Revisiting STAT3 signalling in cancer: new and unexpected biological functions. Nat Rev Cancer 2014; 14: 736-46.

[37] Settembre C, Di Malta C, Polito VA, Garcia Arencibia M, Vetrini F, Erdin S, Erdin SU, Huynh T, Medina D, Colella P, Sardiello M, Rubinsztein DC and Ballabio A. TFEB links autophagy to lysosomal biogenesis. Science 2011; 332: 1429-33.

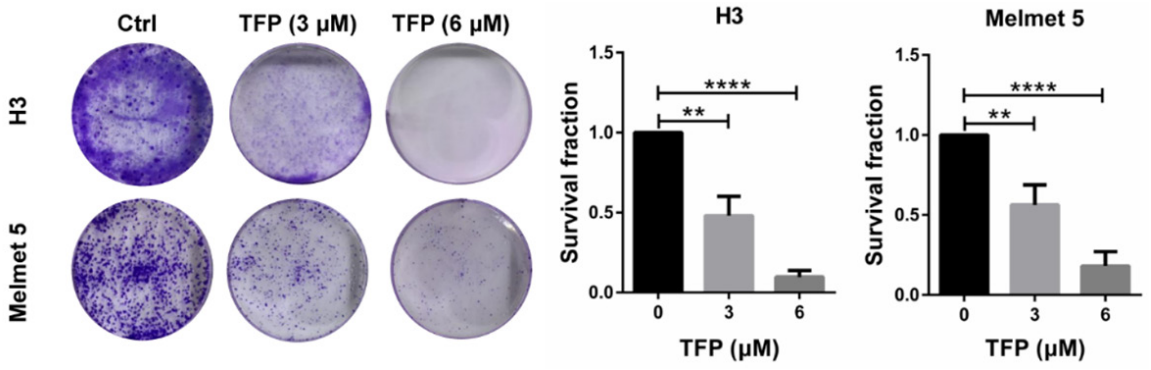

Figure S1. Images and quantification of colony formation assay for H3 and Melmet 5 cells at day 14, after pretreatment with 0 μM (Ctrl), 3 μM or 6 μM TFP for 24 h. **P < 0.01; ****P < 0.0001.

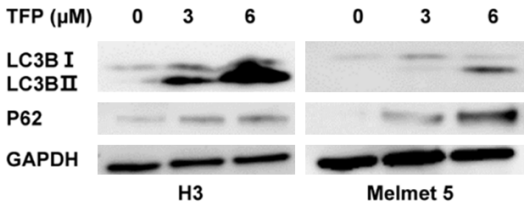

Figure S2. Western blot of LC3B, P62 and GAPDH (loading control) in H3 and Melmet 5 cells treated with 0 μM (Ctrl), 3 μM or 6 μM TFP for 24 h.

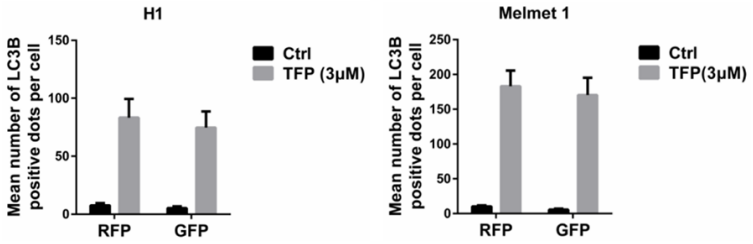

Figure S3. Quantification of autophagic flux in H1 and Melmet 1 cells, 48 h after treatment with either 0 μM (Ctrl) or 3 μM TFP.

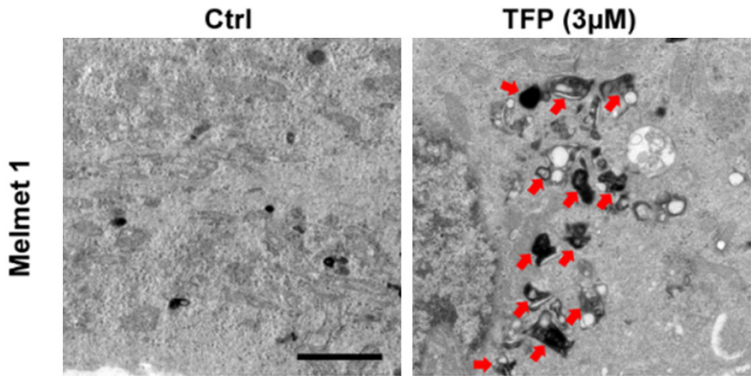

Figure S4. Transmission electron micrographs, showing the ultrastructure of Melmet 1 cells treated with 0 μM (Ctrl) or 3 μM TFP. In TFP treated cells, electron dense vacuoles accumulated (red arrows). Scale bars = 1 μm.

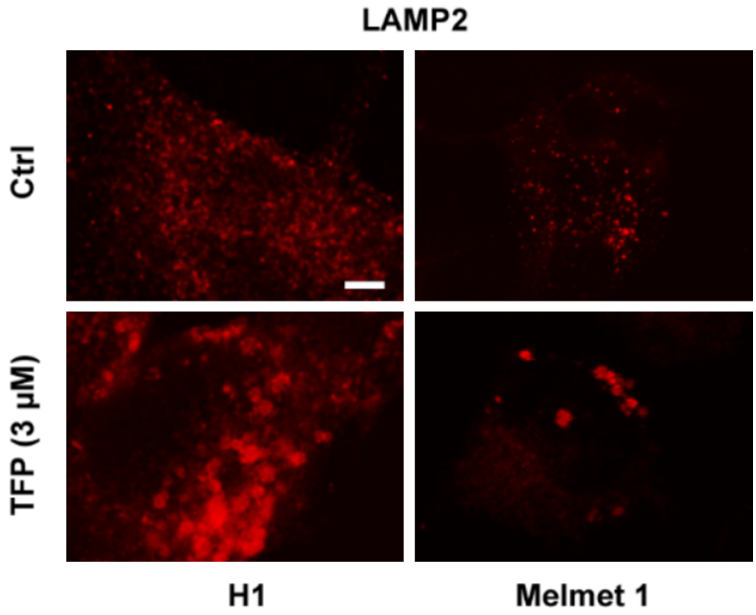

Figure S5. Confocal images showing immunofluorescence staining of the lysosome-associated membrane protein LAMP2 in H1 and Melmet 1 cells, either untreated or treated with 3 µM TFP for 24 h. Scale bar = 10 µm.

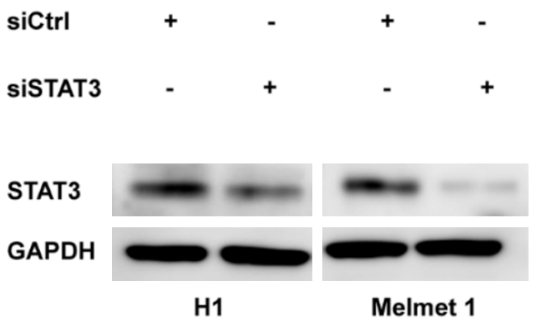

Figure S6. Western blot analysis showing knockdown of STAT3 in H1 and Melmet 1 cells, treated either with siCtrl or with siRNA for STAT3 (siSTAT3).